*materials*

MDPI

*Article*

# Alloying and Hardness of Eutectics with $Nb_{ss}$ and $Nb_5Si_3$ in Nb-silicide Based Alloys

**Panos Tsakiropoulos**

Department of Materials Science and Engineering, University of Sheffield, Sheffield S1 3JD, UK; p.tsakiropoulos@sheffield.ac.uk

Received: 22 March 2018; Accepted: 5 April 2018; Published: 11 April 2018


**Abstract:** In Nb-silicide based alloys, eutectics can form that contain the $Nb_{ss}$ and $Nb_5Si_3$ phases. The $Nb_5Si_3$ can be rich or poor in Ti, the Nb can be substituted with other transition and refractory metals, and the Si can be substituted with simple metal and metalloid elements. For the production of directionally solidified in situ composites of multi-element Nb-silicide based alloys, data about eutectics with $Nb_{ss}$ and $Nb_5Si_3$ is essential. In this paper, the alloying behaviour of eutectics observed in Nb-silicide based alloys was studied using the parameters $\Delta H_{mix}$, $\Delta S_{mix}$, VEC (valence electron concentration), $\delta$ (related to atomic size), $\Delta\chi$ (related to electronegativity), and $\Omega$ (= $T_m \Delta S_{mix} / |\Delta H_{mix}|$). The values of these parameters were in the ranges $-41.9 < \Delta H_{mix} < -25.5$ kJ/mol, $4.7 < \Delta S_{mix} < 15$ J/molK, $4.33 <$ VEC $< 4.89$, $6.23 < \delta < 9.44$, $0.38 < \Omega < 1.35$, and $0.118 < \Delta\chi < 0.248$, with a gap in $\Delta\chi$ values between 0.164 and 0.181. Correlations between $\Delta S_{mix}$, $\Omega$, $\Delta S_{mix}$, and VEC were found for all of the eutectics. The correlation between $\Delta H_{mix}$ and $\delta$ for the eutectics was the same as that of the $Nb_{ss}$, with more negative $\Delta H_{mix}$ for the former. The $\delta$ versus $\Delta\chi$ map separated the Ti-rich eutectics from the Ti-poor eutectics, with a gap in $\Delta\chi$ values between 0.164 and 0.181, which is within the $\Delta\chi$ gap of the $Nb_{ss}$. Eutectics were separated according to alloying additions in the $\Delta\chi$ versus VEC, $\Delta\chi$ versus <Si>, $\delta$ versus <Si>, and VEC versus <Si> maps, where <Si> = Al + Ge + Si + Sn. Convergence of data in maps occurred at $\delta \approx 9.25$, VEC $\approx 4.35$, $\Delta\chi$ in the range $\approx 0.155$ to 0.162, and <Si> in the range $\approx 21.6$ at.% to $\approx 24.3$ at.%. The convergence of data also indicated that the minimum concentration of Ti and maximum concentrations of Al and Si in the eutectic were about 8.7 at.% Ti, 6.3 at.% Al, and 21.6 at.% Si, respectively, and that the minimum concentration of Si in the eutectic was in the range $8 <$ Si $< 10$ at.%.

**Keywords:** eutectic; solid solution; silicide; intermetallic

## 1. Introduction

Nb-silicide based alloys (also known as Nb-silicide in situ composites) are multi-element high temperature alloys. They can offer a balance of properties, and meet property goals to enable future aero engines to comply with new environmental and performance targets [1]. Alloying additions that have been reported in Nb-silicide based alloys include Al, B, Cr, Fe, Ga, Ge, Hf, Ho, Mo, Si, Sn, Ta, Ti, V, W, Y or Zr. The desirable phases in these Nb-Si based alloys are the bcc Nb solid solution ($Nb_{ss}$) and tetragonal $Nb_5Si_3$ silicide. Other phases also can be present, such as for example C14-$NbCr_2$ Laves and A15-$Nb_3X$ intermetallic phases.

In current aero engines, columnar grained and single crystal blades that were manufactured from Ni-based superalloys are used. Eutectic alloys with unusual highly anisotropic microstructures and properties can be manufactured. The properties of directionally solidified (DS) eutectic alloys depend on the regularity and directionality of the microstructure. DS in situ composites can be used at high stress levels at high homologous temperatures, and are capable of meeting the needs of different applications. The evaluation of DS eutectic Nb-silicide in situ composites is desirable.

In situ composites can be produced via liquid-to-solid and solid-to-solid phase transformations. In binary systems with eutectic and eutectoid reactions, in situ composites of the binary eutectics and eutectoids have been studied. The directional solidification of alloys of eutectic composition can produce in situ composites with one or more high strength phases (which are often referred to as reinforcing phases) in a metal matrix. The interface between the matrix and the reinforcing phase is formed at close to equilibrium conditions, and is stable. Microstructures can be stable at high homologous temperatures. Eutectics have been grown with ductile metal matrices and reinforcing whiskers with strengths in excess of 7 GPa [2].

Aligned composites are desirable for high-temperature applications. Those that are grown from the melt have inherent advantages compared with other types of aligned composites, because adequate bonding and low reactivity between the phases is achieved, and there are no lay-up problems or fibre matrix interactions during fabrication.

Aligned in situ composites of near eutectic composition can be fabricated. In binary alloys of compositions well removed from the eutectic, in situ composites have been grown under high G/R ratios, where G is the temperature gradient, and R is the growth rate [3,4]. Multi-component alloys can be grown with a plane front and an aligned composite structure, provided that the interface kinetics do not pose too great a barrier to growth, the G/R ratio is sufficiently high, and the convection is sufficiently low.

DS materials are sensitive to changes in R, G, and composition. Reactions with the mould and core(s) may be a serious problem at low R values. Elements (impurities) of low concentration $C_o$ may influence (i) the stability and (ii) the properties of the DS structure. The effects of such elements may be large (i) because they can cause a macroscopically planar S/L interface to become morphologically unstable. A degeneration of an S/L interface to a non-planar configuration is more pronounced at high R values that produce finer and stronger structures, or low G values. Two ratios, which depend on the processing and alloy parameters, are important. The first is the ratio $G/(RC_o)$, which must be greater than some critical value to produce a controlled DS eutectic. The second is the ratio $(R\Delta T_o/D)$, where $\Delta T_o$ is the freezing range of the alloy, and D is the diffusivity in the melt. For $G < (R\Delta T_o/D)$, the S/L interface becomes morphologically unstable. The value of $\Delta T_o$ depends on composition. $\Delta T_o$ is small when the alloy has the eutectic composition and when the impurity concentration $C_o$ is low. Off-eutectic alloys have larger $\Delta T_o$ values, and impurities also increase $\Delta T_o$. The effects of growth rate fluctuations are minimized for an alloy of eutectic composition. In off-eutectic alloy compositions, growth rate fluctuations cause changes in volume fractions of phases. If the fluctuation in growth rate is large enough, the volume fraction of one phase may go to zero. Thus, knowledge about the composition of the eutectic and element(s) with low concentration (impurities) is essential for regular DS composites. In other words, composites without irregularities in the DS structure, such as change(s) in the cross-section during DS casting, can also change R and G, and thus cause the breakdown of the regular structure.

Research in the early 1970s on titanium matrix eutectics, where Ti was reinforced with an intermetallic phase, reported that reinforcement with 31 vol % $Ti_5Si_3$ fibres gave a considerable improvement of the Young's modulus, compressive yield strength, and creep strength compared with existing commercial alloys [5,6].

The development of Nb-silicide based alloys has concentrated almost exclusively on cast and heat-treated alloys. Powder metallurgy (PM) alloys also have been made [7]. The non-consumable electrode arc melting of small elemental charges (0.01 kg to 0.6 kg) of pure elements in water cooled copper crucibles has been the preferred processing route for the large majority of cast alloys, owing to the limited available facilities and resources for alloy making and processing worldwide.

In the Nb–Si binary phase diagram [8], there are eutectic and eutectoid reactions (see below in this section), which, in principle, make it possible to produce in situ Nb–Si composites via liquid-to-solid and solid-to-solid phase transformations. Research has sought to utilize these reactions for the development of Nb-silicide based alloys [9]. In the 1990s, it was demonstrated that DS in situ Nb–Si

composites can be grown [1,9]. DS Nb-silicide based alloys have been produced using (i) the Bridgman method with liquid metal cooling [10–13], (ii) homemade DS facilities [14–16], and (iii) optical floating zone (OFZ) processing [17–22]. Typical microstructures of DS Nb-silicide based alloys produced using (i) to (iii) are shown in [10–15,17,21].

The fabrication of aligned $Nb_{ss}$ and $Nb_5Si_3$ in situ composites of multi-element Nb-silicide based alloys is highly desirable. Aligned microstructures with $Nb_{ss}$ and $Nb_5Si_3$ could be produced using the directional solidification of eutectics that contain these phases. For the solidification processing of such in situ eutectic composites, data about the eutectics with $Nb_{ss}$ and $Nb_5Si_3$ that can form in Nb-silicide based alloys is required. The following discussion will highlight that such data is currently either non-available or severely limited.

Why it is possible to fabricate in situ composites of Nb-silicide based alloys? Why is there interest in eutectics with $Nb_{ss}$ and $Nb_5Si_3$? To answer these questions, one needs to revisit what is known about eutectic(s) and eutectoid reactions in the Nb–Si binary system. In the Nb-rich part of the equilibrium Nb–Si binary phase diagram, the eutectic and eutectoid reactions are $L \rightarrow Nb_{ss} + Nb_3Si$ (stable eutectic), and $Nb_3Si \rightarrow Nb_{ss} + \alpha Nb_5Si_3$, respectively [8]. The latter is very sluggish. In binary Nb–Si alloys, the former reaction can be suppressed under rapid solidification conditions, and replaced by the metastable eutectic reaction $L \rightarrow Nb_{ss} + \beta Nb_5Si_3$ [23–25]. The phase diagram used in [23] to show the metastable extension of the $Nb_5Si_3$ liquidus to form the metastable eutectic indicated stable eutectic for a liquid composition at Si = 18.7 at.%, and a metastable eutectic at Si $\approx$ 20 at.%. For the stable eutectic in the binary phase diagram, the reported values of the Si concentration of the liquid are in the range 15.3 at.% to 18.7 at.% [26,27]; in other words there is disagreement about the composition of the stable eutectic. There is also disagreement about the temperature of the eutectoid reaction for which the high and low temperatures of 2043 K and 1939 K, respectively, have been reported [28,29]. The concentration of Si in the metastable eutectic estimated from the metastable extension of the $Nb_5Si_3$ liquidus depends on the Nb–Si binary phase diagram that is used.

The tetragonal $Nb_5Si_3$ silicide is preferred for Nb-silicide based alloys owing to its superior properties compared with $Nb_3Si$ and hexagonal $\gamma Nb_5Si_3$. The two phase Nb + $\alpha Nb_5Si_3$ area in the Nb–Si binary has a composition range from 0.6 at.%. to 37.5 at.%. This gives flexibility to form Nb + $Nb_5Si_3$ composites that are stable above the envisaged surface temperature of the new alloys in service ($T_{service} \leq 1673$ K) and with different volume fractions of the phases.

Nb-silicide based alloys have been developed that have met the toughness or creep property goals or significantly closed the gap with the oxidation property goal. These are multi-element Nb–Si-based alloys. Some of the alloying additions provide solid solution strengthening to the $Nb_{ss}$ (for example, Mo, Ta, Ti, and W). Meanwhile, other elements suppress pest oxidation and improve oxidation at high temperatures (for example, Al, B, Cr, Fe, Ge, Hf, Sn, and Ti); other elements suppress the stable eutectic and replace it with the metastable one (for example, Al, Mo, Sn, Ta, and W), and other elements stabilise tetragonal $Nb_5Si_3$ (for example, Al, Cr, Mo, Ta, and W) and improve creep (Mo, Ta, and W). Phase diagrams provide data about eutectic and eutectoid reactions. However, for the design and development of Nb-silicide based alloys, such data is limited. For example, there are no phase diagrams for the Nb-Si-Ta, Nb-Si-Y ternary systems [30], no or limited data about the liquidus projections of the Nb-Si-Al, Nb-Si-Hf, Nb-Si-Mo, Nb-Si-V, Nb-Si-W, Nb-Si-Zr ternary systems [30], and there are disagreements about the Nb-Ti-Si and Nb-Cr-Si liquidus projections [31–37].

Recently, the alloying of $Nb_{ss}$ and tetragonal $Nb_5Si_3$ was reported in [38,39]. The study of the solid solution [38] used the parameters $\Delta H_{mix}$ (enthalpy of mixing), $\Delta S_{mix}$ (entropy of mixing (VEC (valence electron concentration), $\delta$ (parameter related to atomic size), $\Delta\chi$ (parameter related to electronegativity) and $\Omega = T_m \Delta S_{mix} / |\Delta H_{mix}|$. The capital letter Q was used instead of $\Omega$ for the ratio $T_m \Delta S_{mix} / |\Delta H_{mix}|$ in [38] to avoid confusion with the term $\Omega_{ij}$ in the definition of $\Delta H_{mix}$. The above parameters are used in the study of the so-called high entropy alloys. References for publications on high entropy alloys are given in [38]. In [38], the alloying behaviour of the solid solution was described well by the parameters $\delta$, $\Delta\chi$, and VEC. The study of tetragonal $Nb_5Si_3$ [39] also showed that the

parameters $\Delta\chi$ and VEC described its alloying behaviour, and that the changes of the hardness of the alloyed $Nb_5Si_3$ were related to the VEC parameter.

What can we learn about the Si concentration of eutectics that contain $Nb_{ss}$ and $Nb_5Si_3$ from the available data for Nb-silicide based alloys? For these eutectics, would it be possible to deduce (i) the maximum and minimum concentrations of Si in the eutectic, (ii) the total concentration of simple metal and metalloid elements in the eutectic, (iii) the minimum and maximum concentrations of other alloying additions in the eutectic (see the discussion about $C_o$ and $\Delta T_o$ earlier in this section), (iv) the dependence of the concentration of refractory metals on the Si concentration in the eutectic, and (v) whether the hardness of the eutectics is related to the VEC parameter?

The motivation for the research presented in this paper was to answer the above questions. The structure of the paper is as follows. First, the values of the aforementioned parameters will be given for eutectics with $Nb_{ss}$ and $Nb_5Si_3$, and compared with data for Nb-silicide based alloys and their solid solutions. Then, the relationships between them will be discussed. The focus will then be on relationships between parameters, and the concentration of simple and metalloid elements in the eutectic. Next, the relationships between the concentrations of solute additions and the Si concentration in the eutectic will be discussed. Finally, the hardness of the eutectics will be considered.

## 2. Methodology

The available experimental data for the eutectics with $Nb_{ss}$ and $Nb_5Si_3$ in Nb-silicide based alloys from [40–56] was used to seek out relationships between the parameters $\Delta H_{mix}$, $\Delta S_{mix}$, VEC, $\delta$, $\Delta\chi$, and $\Omega$, and between these parameters and the hardness of eutectics. The actual compositions of eutectics with $Nb_{ss}$ and $Nb_5Si_3$ were the essential requirement in order to calculate the parameters of the eutectic. The equations that were used to calculate the parameters $H_{mix}$, $S_{mix}$, VEC, $\delta$, $\Delta\chi$ and $\Omega$ were given in [38]. The data for the properties of elements was from the same sources as in [38].

All of the eutectics studied in this paper were observed in the cast microstructures of Nb-silicide based alloys that had been prepared using arc melting with non-consumable tungsten electrodes in an inert atmosphere with water-cooled copper crucibles. The phases in the cast microstructures of the alloys were identified using XRD (Siemens D5000, Hiltonbrooks Ltd., Crewe, UK) and JCPDS data (International Centre for Diffraction Data), and quantitative microanalysis [40–56]. For the latter, electron probe microanalysis (EPMA) was used in a JEOL 8600 EPMA (JEOL Ltd., Tokyo, Japan) equipped with energy-dispersive and wavelength-dispersive spectrometers and the Oxford Link INCA software (Oxford Instruments plc, Abingdon, UK). Carefully polished standards of high purity of Nb, Si, and the other alloying element additions (Al, Cr, Fe, Ge, Hf, Mo, Sn, Ta, Ti, V, W, Y, and Zr) were used. At least 10 analyses were performed for each eutectic area in an alloy. Each specimen had been carefully polished, and was not etched. The hardness of eutectics was measured using a CV-430 AAT automatic hardness-testing machine. The load that was used was 10 kg, and was applied for 20 seconds. The indentations were made only on the eutectic areas, and covered a larger area relative to inter-lamellar spacing. At least 10 measurements were taken for each phase. The hardness measurements were taken from eutectics with similar inter-lamellar spacing in the order of micrometres. No new experimental data were created during the course of this study.

Eutectics with $Nb_{ss}$ and $Nb_5Si_3$ have been observed in Nb-silicide based alloys with/out Ti addition, and with simple metal and metalloid element additions and other transition and refractory metal additions. The alloys belong in different alloy systems. Eutectics with $Nb_{ss}$ and $Nb_5Si_3$ have been reported in ternary Nb-Si-X (X = Ga, Ge, Mo, Sn) [43,45,57,58]; quaternary Nb-Si-Hf-X (X = Al, Cr, Sn, W) [40,42,49], Nb-Si-Mo-X (X = Al, W) [21,42], Nb-Si-Ge-X (X = Al, Cr) [47,48], Nb-Ti-Si-X (X = Al, Ge, Sn) [46,59]; quinary Nb-Si-Hf-Sn-Al [49], Nb-Si-Hf-Mo-Ta [41], Nb-Ti-Si-Al-Cr [59], Nb-Ti-Si-Sn-X (X = Al, Cr, Fe, Hf) [44,51,52], Nb-Ti-Si-Al-X (X = Ge, Hf) [48], and Nb-Ti-Si-Mo-W [41,42] alloys; and higher order alloys, such as for example Nb-Ti-Si-Al-Cr-X (X = Ge, Hf, Sn, Ta) [10,12,13,15,19,50,53,60], Nb-Ti-Si-Hf-Mo-W [61], Nb-Ti-Si-W-Ge-Sn-X (X = Mo, Ta) [50,53], Nb-Ti-Si-Al-Cr-Mo-W-Ge-Sn [50,53], Nb-Ti-Si-Al-Cr-Ge-Y [55], Nb-Ti-Si-Al-Cr-Hf-B-Y [14,16], and Nb-Ti-Si-Al-Cr-Hf-Ta-Ho [20] alloys. Eutectics with $Nb_{ss}$ and $Nb_5Si_3$

have been observed in boron containing Nb-silicide based alloys, but there is no data for the chemical composition of such eutectics (see discussion of Figures 6 and 13 in the next section).

Both $Nb_{ss}$ and $Nb_5Si_3$ in Nb-silicide based alloys can be alloyed; for example, Nb-32.4Ti-1.4Si-5.8Cr-2.5Al-2.8Fe-4.9Sn-1.3Hf and Nb-34.1Si-20.7Ti-9.6Hf-3.7Al-1.8V-0.4Cr-0.4Sn are actual average chemical compositions (at.%) respectively of a solid solution and a $Nb_5Si_3$ silicide in two different Nb-silicide based alloys. Some of the alloying additions partition preferably to one of these phases (for example, Sn partitions to the $Nb_{ss}$ [43,44] and Ge partitions to the $Nb_5Si_3$ [45–48]) and other elements partition to both phases (for example, Hf and Ti). Depending on alloying additions, other phases also can form, for example A15-$Nb_3X$ (X = Al, Ge, Sn, Si) and C14-$NbCr_2$ Laves. These phases also are alloyed; for example, Nb-25.4Ti-2.3Cr-0.7Fe-0.3Hf-10.9Sn-5.1Si-2.4Al [52] and Nb-6.6Ti-6.9Ta-4.4W-1.1Hf-44.2Cr-8.7Si-6Al-1Ge-0.6Sn [50] are actual average chemical compositions (at.%) respectively of an A15 and a Laves phase in two different Nb-silicide based alloys.

The A15 phases are observed next to the $Nb_{ss}$, and the Laves phases form in the last to solidify Cr-rich melt in between $Nb_{ss}$ and $Nb_5Si_3$ dendrites [59,60]. Under backscatter electron (BSE) imaging conditions, the contrasts of $Nb_{ss}$ and A15-$Nb_3X$ phase are similar. Ti-rich areas can form in $Nb_{ss}$ and $Nb_5Si_3$. $Nb_{ss}$/$Nb_5Si_3$ interfaces also can be Ti-rich. In Hf and Ti-containing alloys, the increase of the concentration of Ti in $Nb_{ss}$ and/or $Nb_5Si_3$ is accompanied by an increase of the concentration of Hf. In alloys with Mo and W additions, the partitioning of these elements and Ti in the $Nb_{ss}$ also creates problems with contrast, as Mo and W "do not like Ti in the $Nb_{ss}$", meaning that as the concentrations of Mo and W increase, that of Ti decreases. The variations in contrast that arise from the partitioning of solutes and the fine microstructures of the eutectics sometimes made it very difficult to confirm whether a binary $Nb_{ss}$ + $Nb_5Si_3$ or a ternary eutectic between $Nb_{ss}$ and $Nb_5Si_3$ and A15-$Nb_3X$ or C14-$NbCr_2$ Laves had formed in alloys with three or more phases. In the great majority of the alloys studied in this paper binary, $Nb_{ss}$ + $Nb_5Si_3$ eutectics were observed. All of the eutectics studied in this paper contained $Nb_{ss}$ and $Nb_5Si_3$. No eutectics that contained $Nb_{ss}$ and $Nb_3Si$ were studied in this paper.

The experimental data [40–56] about the actual average chemical compositions of the eutectics with $Nb_{ss}$ and $Nb_5Si_3$ observed in alloys of the aforementioned systems was used to study the alloying behaviour of the eutectic. Compositions of eutectics with $Nb_{ss}$ and $Nb_5Si_3$ are given in [40–56]. The eutectics had 1.9 < Al < 6.4 at.%, 1.3 < Cr < 7.7 at.%, 1.2 < Ge < 7.8 at.%, Hf < 8.6 at.%, 1.2 < Mo < 11.3 at.%, 8.1 < Si < 24.4 at.%, 1.2 < Sn < 5.4 at.%, 8.2 < Ti < 36.8 at.%, and 2 < W < 5.8 at.%. The total concentration of simple element and metalloid element additions in the eutectic is given in this paper as <Si> = Al + Ge + Si + Sn; i.e., the <Si> (at.%) includes the additions of Al, Ge, Si, and Sn, depending on whether Al, Ge, and Sn were present individually or simultaneously in the alloy.

## 3. Results and Discussion

The ranges of the values of the aforementioned parameters for the eutectics with $Nb_{ss}$ and $Nb_5Si_3$ are given in Table 1, where they are compared with those of the Nb-silicide based alloys [62] and $Nb_{ss}$ in all of the alloys [38]. As was the case in [62], the parameters were not used to predict whether the eutectics are HEAs (high entropy alloys) or whether the solid solution and/or intermetallic(s) will be stable. They were used to study alloying behaviour in the eutectics, discover if there are relationships between parameters and between parameters and solute concentrations in eutectics, and find out if the hardness of eutectics is related to specific properties. Compared with Nb-silicide based alloys [62], the eutectics had wider ranges of $\Delta H_{mix}$, $\Delta S_{mix}$, $\Delta\chi$, and $\Omega$ values, the VEC range was essentially the same, the range of $\delta$ values was narrow, and some eutectics had $\delta$ values that were lower than those in the Nb-silicide based alloys. Compared with Nb solid solutions [38], the eutectics had more negative $\Delta H_{mix}$ values with a wider range, the $\Delta S_{mix}$ range was slightly wider, the ranges of the VEC, $\Delta\chi$, and $\delta$ values were narrow and in the ranges of the values of $Nb_{ss}$ in all of the alloys, and the $\Omega$ values were smaller and outside the $\Omega$ range of the solid solution.

**Table 1.** Values of the parameters $\Delta H_{mix}$, $\Delta S_{mix}$, valence electron concentration (VEC), δ, Δχ, and Ω for all of the Nb-silicide based alloys and their solid solutions, and for the eutectics with $Nb_{ss}$ and $Nb_5Si_3$.

| Material | Parameter | | | | | |
|---|---|---|---|---|---|---|
| | **$\Delta H_{mix}$/(kJ/mol)** | **$\Delta S_{mix}$ (J/molK)** | **VEC** | **δ** | **Δχ** | **Ω +** |
| Nb-silicide based alloys [62] | −32.7 to –44.8 | 8.3–14.7 | 4.37–4.9 | 8.1–14.3 | 0.12–0.237 | 0.57–0.95 |
| $Nb_{ss}$ in Nb-silicide based alloys [38] | −2 to –15.9 | 5.8–14.5 | 4.4–5.4 | 2.4–9.7 | 0.039–0.331 with a gap in the range 0.13 to 0.179 | 1.55–8.9 |
| Eutectics with $Nb_{ss}$ and $Nb_5Si_3$ | −25.5 to –41.9 | 4.7–15 | 4.33–4.89 | 6.23–9.44 | 0.118–0.248 with a gap in the range 0.164 to 0.181 | 0.38–1.35 |

+ The capital letter Q was used instead of Ω for the ratio $T_m\Delta S_{mix} / |\Delta H_{mix}|$ in [38].

Figures 1 and 2 show the relationship between the parameters $\Delta S_{mix}$ and Ω, and $\Delta S_{mix}$ and VEC of the eutectics, respectively. Figure 1 shows that the $\Delta S_{mix}$ increases with Ω. All of the available data exhibits a linear fit with $R^2 = 0.8133$, and the data subsets of the eutectics that contain only Sn (meaning <Si> = Al + Si + Sn) or only Ge (<Si> = Al + Ge + Si) exhibit better linear fits with $R^2$ values of 0.8754 and 0.9863, respectively. Such a relationship was not exhibited by the $\Delta S_{mix}$ and Ω parameters of the $Nb_{ss}$.

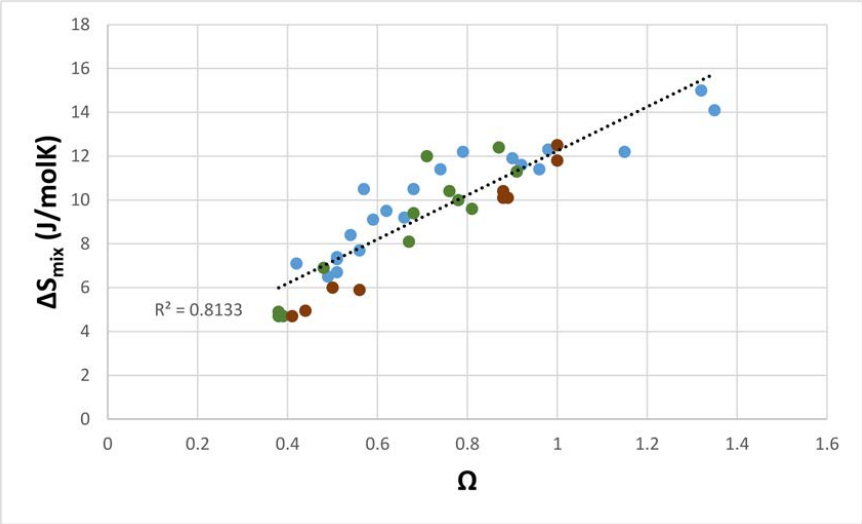


**Figure 1.** $\Delta S_{mix}$ versus Ω of eutectics with $Nb_{ss}$ and $Nb_5Si_3$ in Nb-silicide based alloys, all data $R^2 = 0.8133$, eutectics with only Sn (filled green circles) $R^2 = 0.8754$, eutectics with only Ge (filled brown circles) $R^2 = 0.9863$.

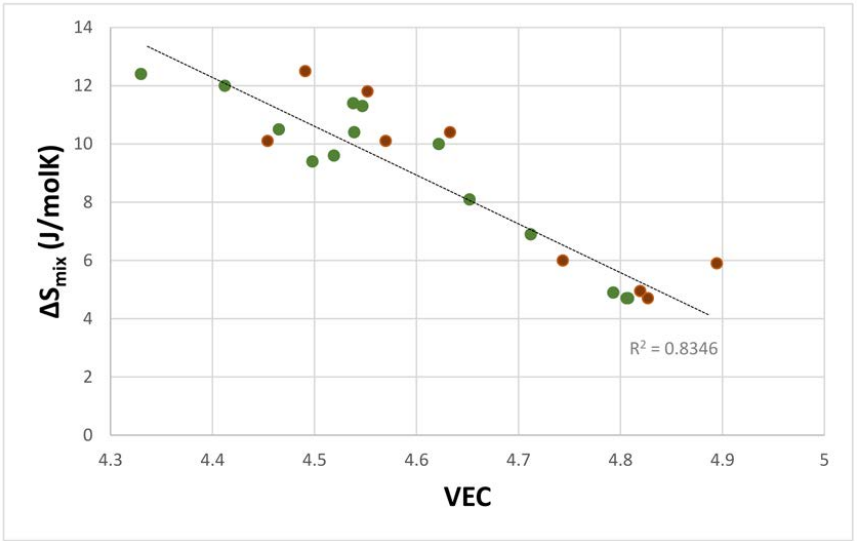


**Figure 2.** $\Delta S_{mix}$ versus VEC of eutectics with $Nb_{ss}$ and $Nb_5Si_3$ in Nb-silicide based alloys with only Ge or Sn. All of the data $R^2 = 0.8346$, eutectics with only Sn (filled green circles) $R^2 = 0.8966$, eutectics with only Ge (filled brown circles) $R^2 = 0.8183$.

Figure 2 shows that the VEC parameter increases with the decreasing $\Delta S_{mix}$ of the eutectic. The data in this figure is for eutectics in alloys with only a Ge or only an Sn addition. All of the data exhibits a linear fit with $R^2 = 0.8346$. The linear fit for the eutectics with only Sn (green circles) or only Ge (brown circles), respectively, gives $R^2 = 0.8966$ and $R^2 = 0.8183$. Similar behaviour was not observed for the parameters VEC and $\Delta S_{mix}$ of the $Nb_{ss}$.

The $\Delta H_{mix}$ of the $Nb_{ss}$ decreases (becomes more negative) as the parameter δ increases [38]. The same trend was found for the eutectics, see Figure 3. In Figure 3, the linear fit of all of the data is good ($R^2$ = 0.8925), the data for the eutectics follows the trend of the data for the $Nb_{ss}$, and the gap in the $\Delta H_{mix}$ values is shown by the horizontal dashed lines. There was also good correlation of the data in $\Delta H_{mix}$ versus Ω ($R^2$ = 0.8485), and Ω versus Δχ ($R^2$ = 0.8515) plots (Figures not shown) for eutectics where Ge and Sn were present simultaneously (meaning <Si> = Al + Ge + Si + Sn).

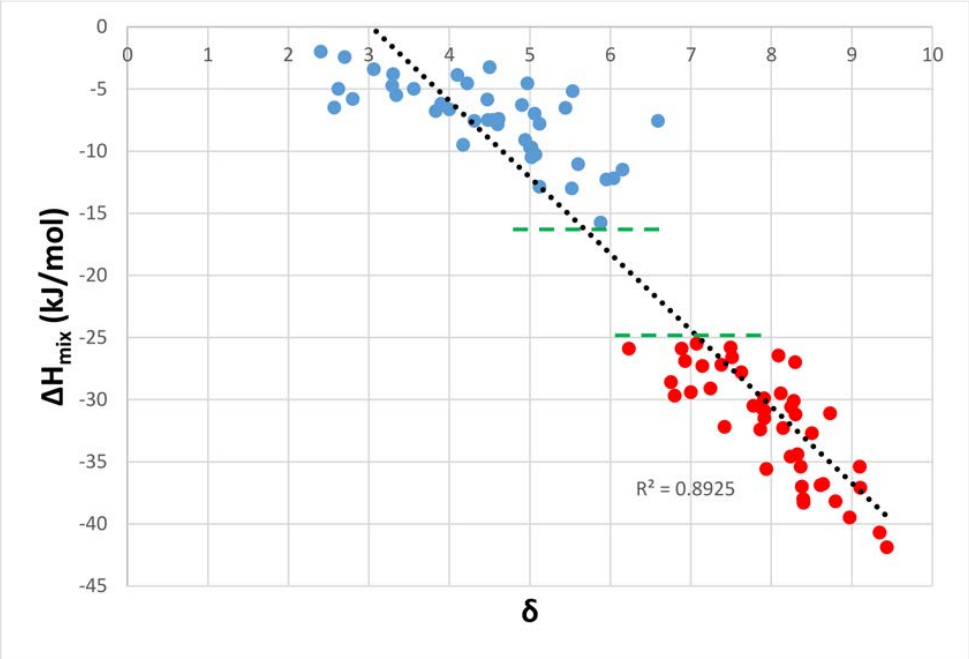


**Figure 3.** $\Delta H_{mix}$ versus δ of $Nb_{ss}$ (filled blue circles) and of eutectics with $Nb_{ss}$ and $Nb_5Si_3$ (filled red circles) in Nb-silicide based alloys. All of the data linear fit with $R^2$ = 0.8925.

The δ versus Δχ map of the eutectics is shown in Figure 4. The partitioning of Ti in the Nb-silicide based alloys is important for the chemical composition and properties of the $Nb_{ss}$ and $Nb_5Si_3$. For example, Ti and Cr, and Ti and Hf "like each other" in the $Nb_{ss}$ and $Nb_5Si_3$ (meaning the concentrations of Cr and Hf increase with increasing Ti concentration in the solid solution and the silicide) but not Ti, Mo, and W in the $Nb_{ss}$, in which as the Ti concentration increases, those of Mo and W decrease. The δ versus Δχ map separates the Ti-rich eutectics from the Ti-poor ones, and shows a gap in Δχ values between the two groups (note that in cast Nb-silicide based alloys with Ti additions, it is possible to form Ti-rich $Nb_{ss}$ and Ti-rich $Nb_5Si_3$, [59,60]). The gap in Δχ values of the eutectics falls in the gap of Δχ values of the $Nb_{ss}$ (Table 1). However, the δ versus Δχ map cannot separate the contributions made by different groups of alloying additions. This is possible in the Δχ versus VEC map of the eutectics, which is shown in Figure 5. The eutectics, whose data points fall in the gap of the Δχ values of the $Nb_{ss}$, belonged in alloys where only normal $Nb_{ss}$ was formed [38]. The alloying elements in each data series in Figure 5 are indicated in the figure caption. In the series a, as well as in the series c to f, there is no Fe; there is no Ge in series f; there is no Mo in series a, b, and g; there is no Ta in series a, b, e, and g; there is no V in series a, b, e, and g; there is no W in series a, b, f, and g; and Zr is only in series c. It should be noted that the linear fits of the data "converge" to VEC ≈ 4.35 and Δχ ≈ 0.162. The "convergence" of the data suggested that alloying elements in the eutectics in Nb-silicide based alloys might have minimum and maximum concentrations. This was confirmed by further analysis of the data for the eutectics, as shown below.

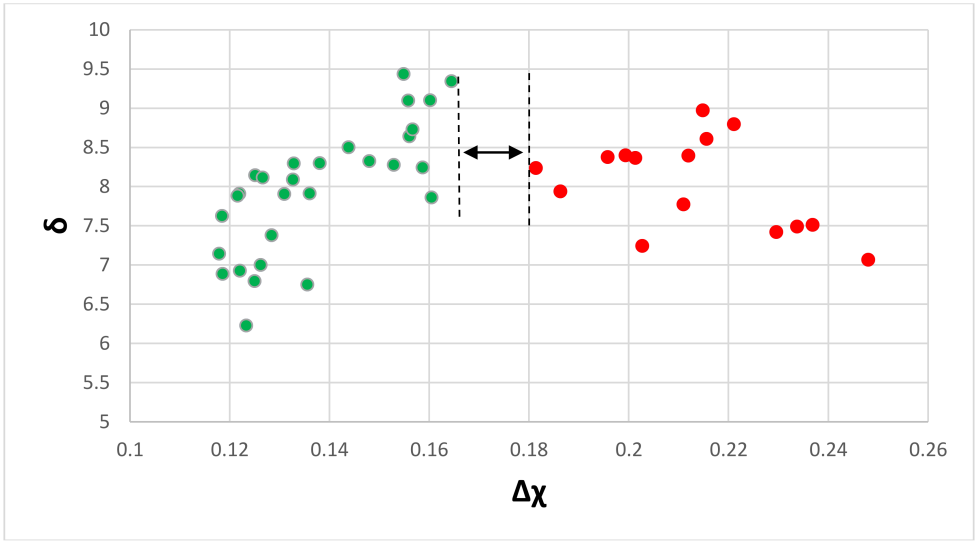


**Figure 4.** δ versus Δχ of eutectics with $Nb_{ss}$ and $Nb_5Si_3$ in Nb-silicide based alloys. The gap in Δχ values ($0.164 < \Delta\chi < 0.181$) separates eutectics with low Ti concentrations ($8.3 < Ti < 13.5$ at.%), which are shown with filled red circles, from those of high Ti concentration ($20.5 < Ti < 45$ at.%), which are shown with filled green circles.

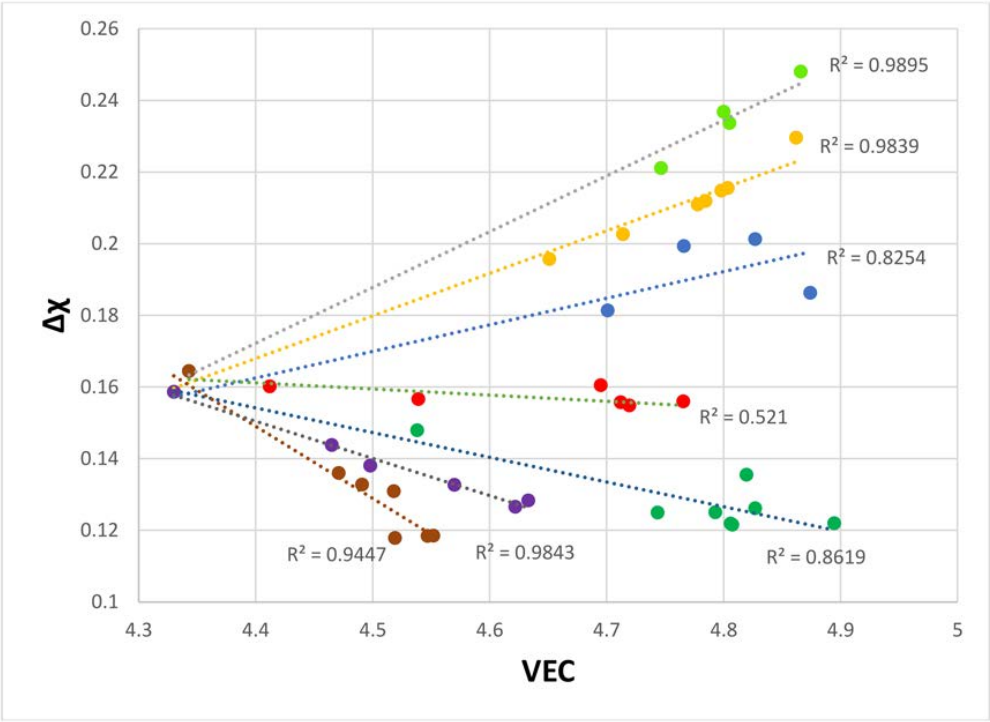


**Figure 5.** Δχ versus VEC of eutectics with $Nb_{ss}$ and $Nb_5Si_3$ in Nb-silicide based alloys. Series a ($R^2 = 0.9447$) with alloying element additions of Al, Cr, Ge, Hf, Si, Sn, Ti, and Y; series b ($R^2 = 0.9843$) with alloying element additions of Al, Cr, Fe, Ge, Si, Sn, and Ti; series c ($R^2 = 0.8254$) with alloying element additions of Al, Cr, Ge, Hf, Mo, Si, Sn, Ta, Ti, V, W, and Zr; series d ($R^2 = 0.9893$) with alloying element additions of Al, Cr, Ge, Hf, Mo, Si, Sn, Ta, Ti, V, and W; series e ($R^2 = 0.9895$) with alloying element additions of Al, Cr, Ge, Hf, Mo, Si, Sn, Ti, and W; series f ($R^2 = 0.5210$) with alloying element additions of Al, Cr, Hf, Mo, Si, Sn, Ta, Ti, and V; series g ($R^2 = 0.8619$) with alloying element additions of Al, Cr, Fe, Ge, Hf, Si, Sn, and Ti.

The dependence of the parameter $\Delta\chi$ on the <Si> of the eutectics is shown in Figure 6. The data falls in different subsets, the alloying elements of which are given in the figure caption. All of the subsets "converge" to <Si> ≈ 21.6 at.% and $\Delta\chi \approx 0.155$. Series b and e have no Fe; there is no Mo, no Ta and no W in series a, b and e; the elements V and Zr are only in series c, and Y is only in series a and e. The trend between $\Delta\chi$ and <Si> for series c and d is the same as that of the parameter $\Delta\chi$, and the sum of simple metal and metalloid element additions in $Nb_5Si_3$, as shown in Figure 7. Figure 7 has data for the $Nb_5Si_3$ in Nb-silicide based alloys with/out eutectics, not for $Nb_5Si_3$ in eutectics. It should be noted that (i) the data in Figure 7 includes boron-containing silicides (their data falls on the same trend as for the other simple metal and metalloid elements) and (ii) there is no data for the chemical composition of eutectics with $Nb_{ss}$ and $Nb_5Si_3$ in boron-containing alloys (see Section 2). The data for the $\Delta\chi$ and $<Si>_{Nbss}$ of the $Nb_{ss}$, where $<Si>_{Nbss}$ = Al + Ge + Si + Sn, showed that the $\Delta\chi$ of the $Nb_{ss}$ can increase or decrease with increasing $<Si>_{Nbss}$, depending on alloying element additions. This would suggest that in the eutectics of the series c and d in Figure 6, the composition of the eutectics was "controlled" by the silicide. Similarities between the alloying elements in the different series in Figures 5 and 6 should be noted.

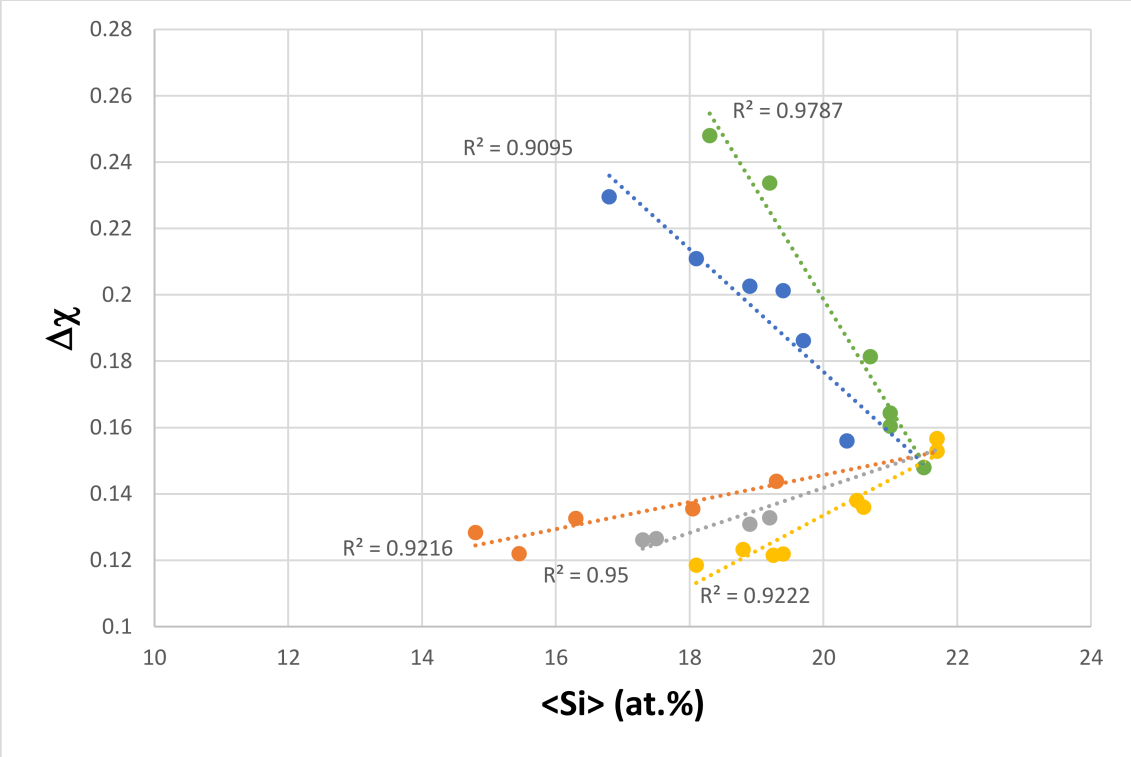


**Figure 6.** $\Delta\chi$ versus <Si> of eutectics with $Nb_{ss}$ and $Nb_5Si_3$ in Nb-silicide based alloys. Series a ($R^2$ = 0.9216) with alloying element additions of Al, Cr, Fe, Ge, Hf, Si, Sn, Ti, and Y; series b ($R^2$ = 0.9222) with alloying element additions of Al, Cr, Ge, Hf, Si, Sn, and Ti; series c ($R^2$ = 09095) with alloying element additions of Al, Cr, Fe, Ge, Hf, Mo, Si, Sn, Ta, Ti, V, W, and Zr; series d ($R^2$ = 0.9787) with alloying element additions of Al, Cr, Fe, Ge, Hf, Mo, Si, Sn, Ta, Ti, and W; series e ($R^2$ = 0.95) with alloying element additions of Al, Cr, Ge, Hf, Si, Sn, Ti, and Y.

The dependence of δ on the <Si> of the eutectic is shown in Figure 8. The data falls in different subsets, the alloying elements of which are given in the figure caption. Series b and d have no Fe, there is no Mo in series d, there is no Ta in series a, there is no V in series d, and Y and Zr are only present in series c. All of the series "converge" to <Si> ≈ 24.35 at.% and δ ≈ 9.25 The parameter δ increases with increasing <Si> for all of the series. Similarities between the alloying elements in the different series in Figures 5, 6 and 8 should be noted.

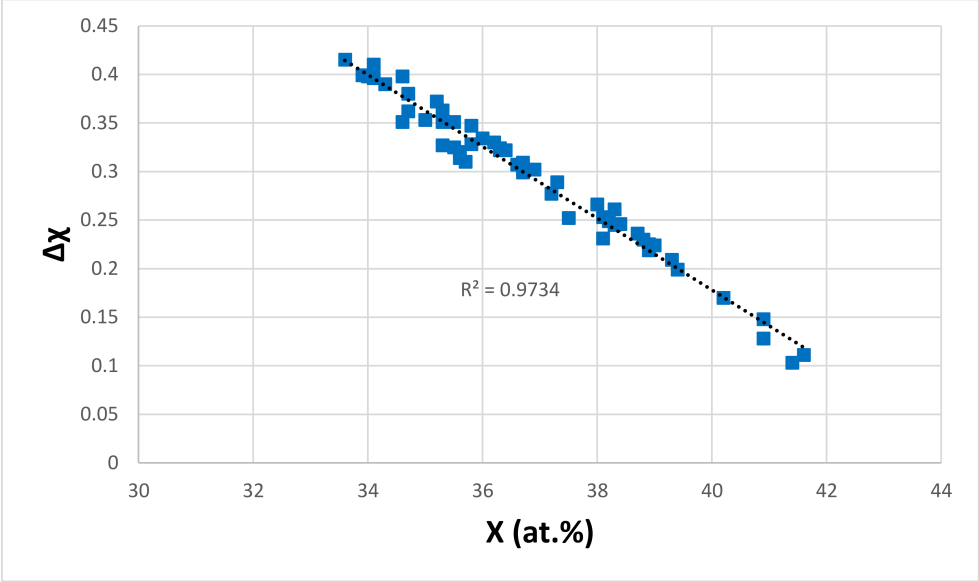


**Figure 7.** Δχ of tetragonal $Nb_5Si_3$ versus X (= Al + B + Ge + Si + Sn) in $Nb_5Si_3$ in Nb-silicide based alloys, see text.

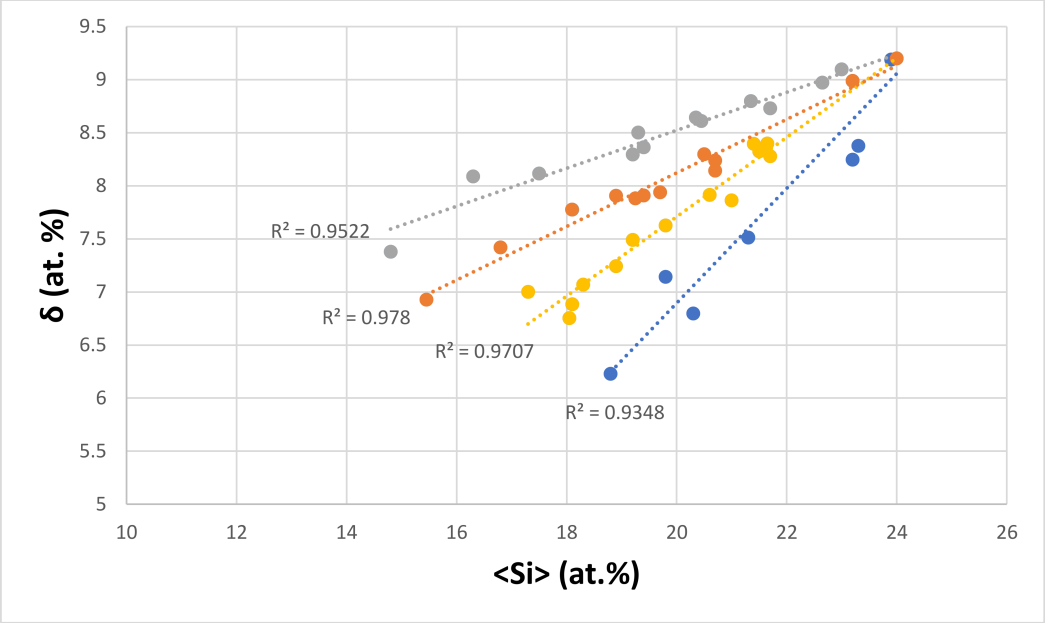


**Figure 8.** δ versus <Si> of eutectics with $Nb_{ss}$ and $Nb_5Si_3$ in Nb-silicide based alloys. Series a ($R^2$ = 0.9707) with alloying element additions of Al, Cr, Fe, Ge, Hf, Mo, Si, Sn, Ti, V, and W; series b ($R^2$ = 0.9348) with alloying element additions of Al, Cr, Ge, Hf, Si, Sn, Ta, Ti, V, and W; series c ($R^2$ = 0.9522) with alloying element additions of Al, Cr, Fe, Ge, Hf, Mo, Si, Sn, Ta, Ti, V, W, Y, and Zr; and series d ($R^2$ = 0.978) with alloying element additions of Al, Cr, Ge, Hf, Mo, Si, Sn, Ta, Ti, and W.

Titanium is an important addition in Nb-silicide based alloys, because it improves oxidation and toughness, and reduces density. It partitions to $Nb_{ss}$ and $Nb_5Si_3$ [59,60] where its concentration affects that of other elements. Both phases can have Ti-rich areas that persist only in the silicide after exposure to high temperatures [59,60]. The relationship between the Ti and Si concentrations of the eutectics is shown in Figure 9. The data falls into four subsets, of which series d has no Al and Cr. All four series "converge" to Si ≈ 21.6 at.% and Ti ≈ 8.7 at.%, and show that the Si concentration in

the eutectic decreases as the Ti concentration increases. The latter was also the case for the Ti and Si concentrations in $Nb_5Si_3$ in Nb-silicide based alloys with/out eutectics, but not for the $Nb_{ss}$ where the Si concentration increases as the Ti concentration increases.

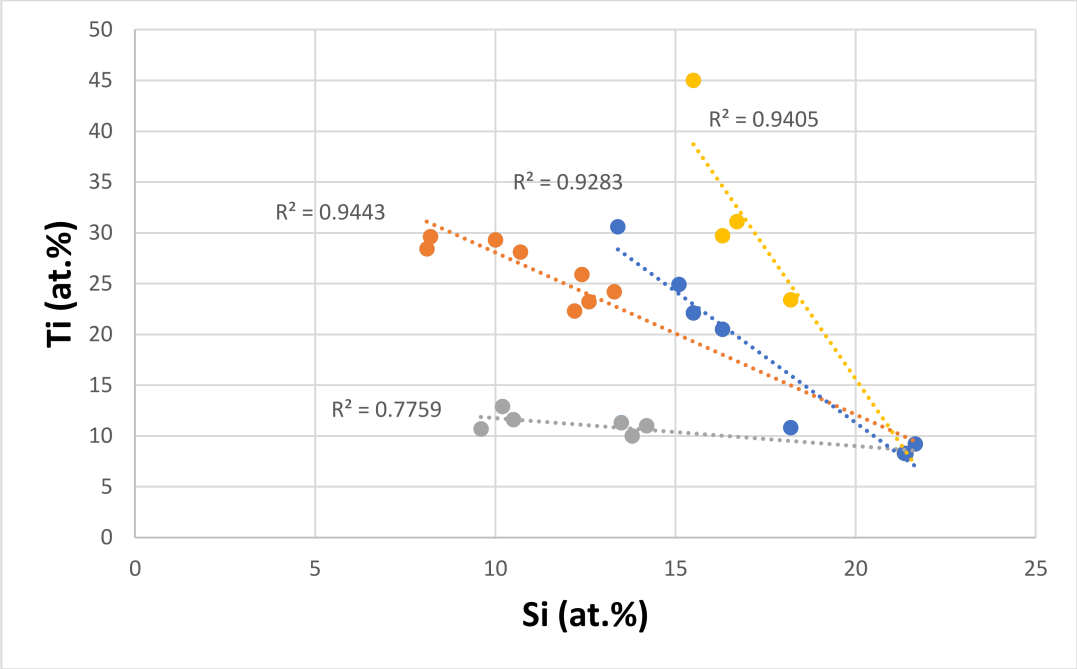


**Figure 9.** Ti versus Si of eutectics with $Nb_{ss}$ and $Nb_5Si_3$ in Nb-silicide based alloys, series a ($R^2$ = 0.9443), with alloying element additions of Al, Cr, Ge, Hf, Mo, Si, Sn, Ti, W, and Y; series b ($R^2$ = 0.7759) with alloying element additions of Al, Cr, Ge, Hf, Mo, Si, Sn, Ti, V, and W; series c ($R^2$ = 0.9405) with alloying element additions of Al, Cr, Fe, Hf, Mo, Si, Sn, Ti, V, and W; series d ($R^2$ = 0.9283) with alloying element additions of Ge, Hf, Mo, Si, Sn, Ta, Ti, and W.

Aluminium is added at low concentrations in Nb-silicide based alloys because of its adverse effect on their toughness. It reduces density and contributes to the improvement of oxidation resistance with additions of B, Ge, or Sn. It partitions to $Nb_{ss}$ and $Nb_5Si_3$, where its concentration depends on other alloying elements [59,60]. Figure 10 shows the relationship between the Al and Si concentrations of the eutectics. The data falls in three subsets, with the alloying elements in each series indicated in the figure caption. All of the subsets of data show that as the Si concentration in the eutectic decreases, the Al content increases, which is in agreement with the data for $Nb_5Si_3$ in Nb-silicide based alloys with/out eutectics, but not with the data for the $Nb_{ss}$. The data "converges" to Al ≈ 6.3 at.% and Si ≈ 8 at.%. Similarities between the alloying elements in the different series in Figures 9 and 10 should be noted.

In Nb-silicide based alloys, Hf is added to improve the oxidation and toughness and scavenge oxygen to form hafnia. Hafnium partitions to both the $Nb_{ss}$ and $Nb_5Si_3$, and its concentration is related to that of Ti in the two phases. The Hf concentration decreases with decreasing Si concentration in eutectics, and the data "converges" to Hf ≈ 1 at.% and Si ≈ 10 at.%. The trend of the data (figure not shown) is the same as that of the Hf and Si concentrations in the $Nb_{ss}$ in Nb-silicide based alloys with/out eutectics. There is no correlation between the Hf and Si concentrations in $Nb_5Si_3$.

The "convergence" of data that was shown earlier would suggest that (i) the alloying elements have maximum and minimum concentrations in the eutectics, and (ii) the maximum concentrations of Al and Si in the eutectic are about 6.3 at.% and 21.6 at.%, respectively. The minimum concentration of Ti in the eutectic is about 8.7 at.%, and the minimum concentration of Si in the eutectic is in the range of 8 at.% to 10 at.%.

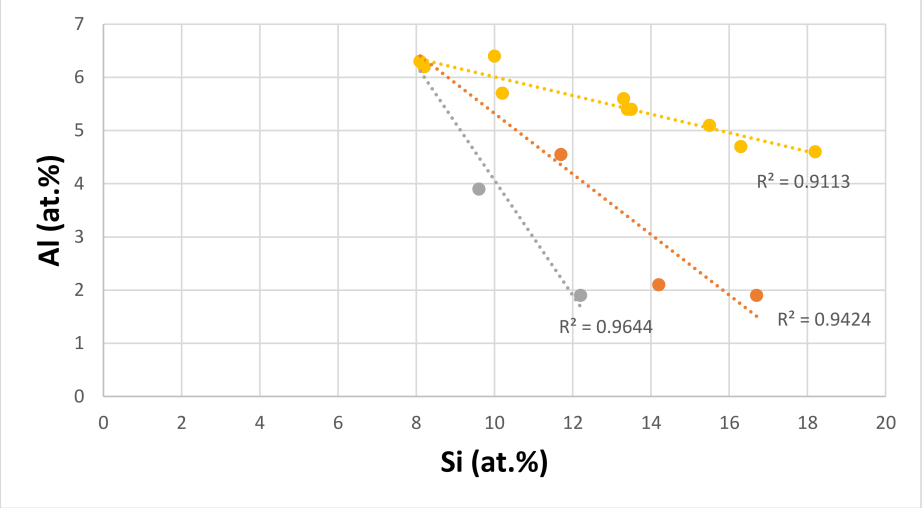


**Figure 10.** Al versus Si of eutectics with $Nb_{ss}$ and $Nb_5Si_3$ in Nb-silicide based alloys, series a ($R^2$ = 0.9644) with alloying element additions of Al, Cr, Ge, Hf, Mo, Si, Sn, Ti, W, and Y; series b ($R^2$ = 0.9113) with alloying element additions of Al, Cr, Ge, Hf, Mo, Si, Sn, Ti, V, W, and Y; series c ($R^2$ = 0.9424) with alloying element additions of Al, Cr, Fe, Ge, Hf, Mo, Si, Sn, Ti, and W.

The refractory metals Mo, Ta, and W can be present in the eutectics, and can stabilise their lamellar microstructure at high temperatures, depending on the other alloying additions in the Nb-silicide based alloy [41,42,50,53,60,61]. Their concentration in the eutectic also is related to the Si concentration of the latter. Molybdenum is chosen to demonstrate this relationship in this paper. Figure 11 shows that the Mo concentration of the eutectics decreases as the Si concentration increases. This is consistent with the data for the $Nb_{ss}$ in Nb-silicide based alloys with/out eutectics, which shows the same trend, and also with the partitioning behaviour of Ti and Mo in the solid solution where, as the Ti concentration increases, the Mo concentration decreases.

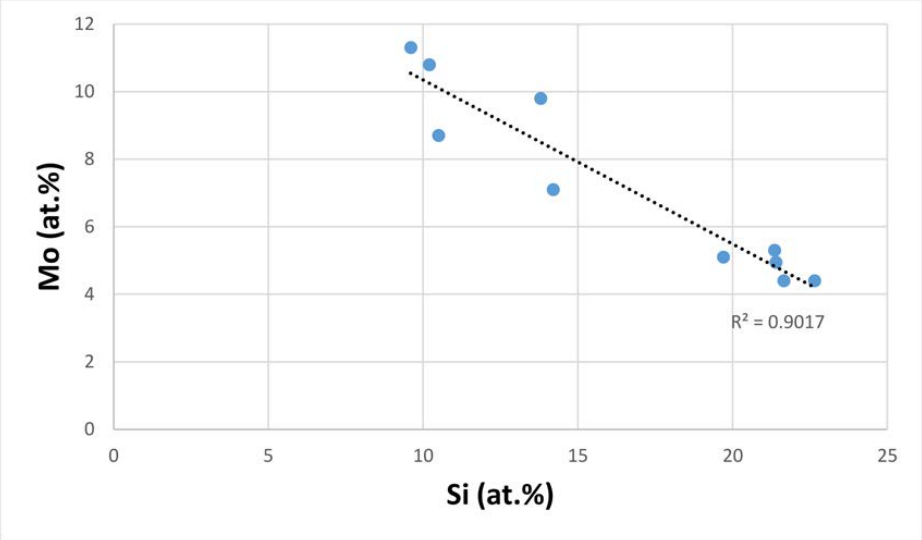


**Figure 11.** Mo versus Si of eutectics with $Nb_{ss}$ and $Nb_5Si_3$ in Nb-silicide based alloys, elements in eutectics: Al, Cr, Ge, Hf, Mo, Nb, Si, Sn, Ti, and W.

Data for the hardness of eutectics with $Nb_{ss}$ and $Nb_5Si_3$ is available for the Nb-silicide based alloys without the addition of Ti, and are shown in Figure 12. The eutectics were observed in alloys of the following systems: Nb-Si-Sn, Nb-Si-Ge, Nb-Si-Hf-Al, Nb-Si-Hf-Sn, Nb-Si-Ge-Al,

and Nb-Si-Cr-Ge [40,43,45,47–49]. The eutectics in the alloys in Figure 12 had <Si> = Si + Sn, <Si> = Si + Al, <Si> = Si + Ge, or <Si> = Si + Al + Ge. The microstructures of the Sn-containing alloys consisted of three phases, namely $Nb_{ss}$, $Nb_5Si_3$, and A15-$Nb_3Sn$, and the microstructures of the alloys without Sn addition contained only $Nb_{ss}$ and $Nb_5Si_3$. The data points for the alloys with A15-$Nb_3Sn$ in their microstructures are indicated in the blue colour in Figure 12. Figure 12a shows that the hardness of the eutectics increased as the VEC increased. The same trend between hardness and VEC was observed for the hardness of the A15-$Nb_3X$ phases in the Nb-silicide based alloys [63], for $\beta(Nb,Ti)_5Si_3$ (see below), and for the hardness of tetragonal $Nb_5Si_3$, as shown in Figure 13. Note that the data in the latter figure is for the $Nb_5Si_3$ in Nb-silicide based alloys, not for the $Nb_5Si_3$ lamellae in eutectics with $Nb_{ss}$ and $Nb_5Si_3$ in such alloys. The elements in each data series in Figure 13 are given in the caption. Mo is only in series c; W is only in series d, which does not also have B, Ge, and Ta; V is not in series a and b; and there is no Sn in series b. Eutectics with $Nb_{ss}$ and $Nb_5Si_3$ have been observed in boron-containing Nb-silicide based alloys. There is data for the chemical composition and hardness of the 5-3 silicide in the microstructure of the latter, but not for the eutectics (see Section 2).

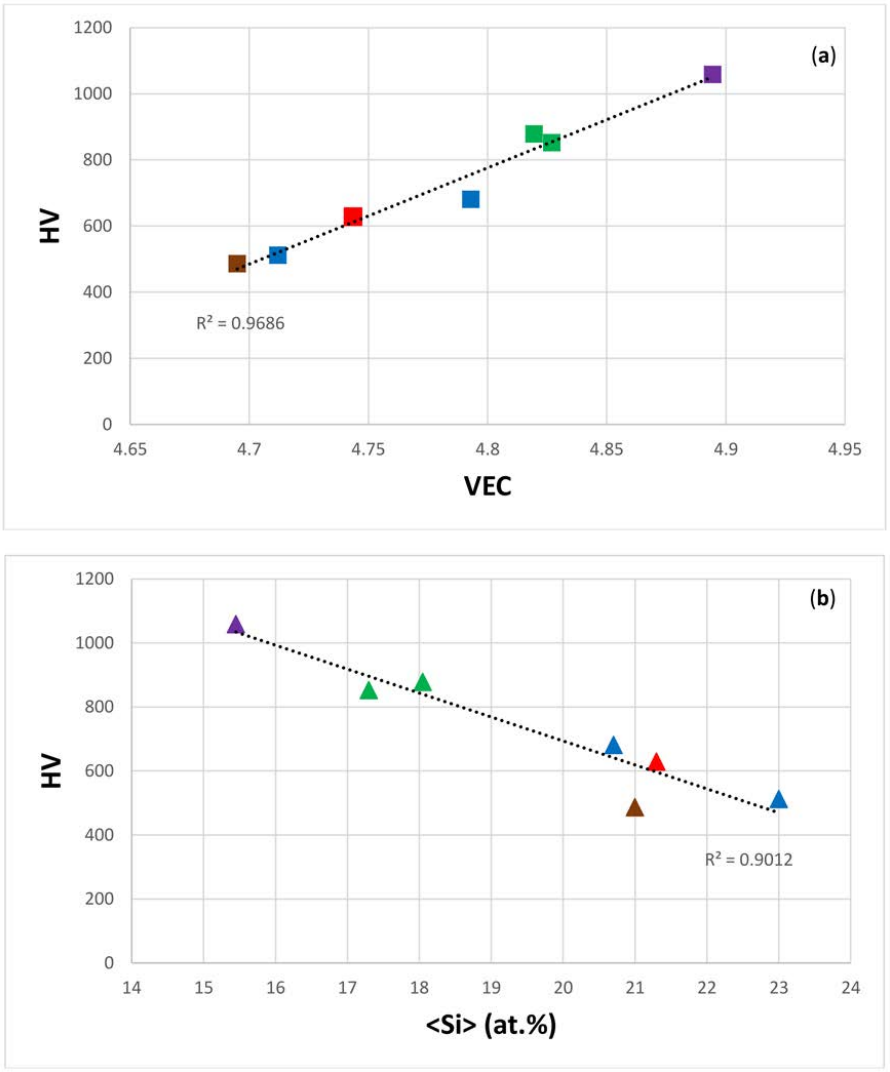


**Figure 12.** Average Vickers hardness of eutectics versus (**a**) VEC and (**b**) <Si> of eutectics. In both (**a**,**b**), data for the eutectics with Sn is shown in blue, data for the eutectics with Al is shown in brown, data for the eutectics with Al and Ge is shown in red, data for the eutectics with Ge is shown in green, and data for the eutectics with Cr and Ge is shown in purple.

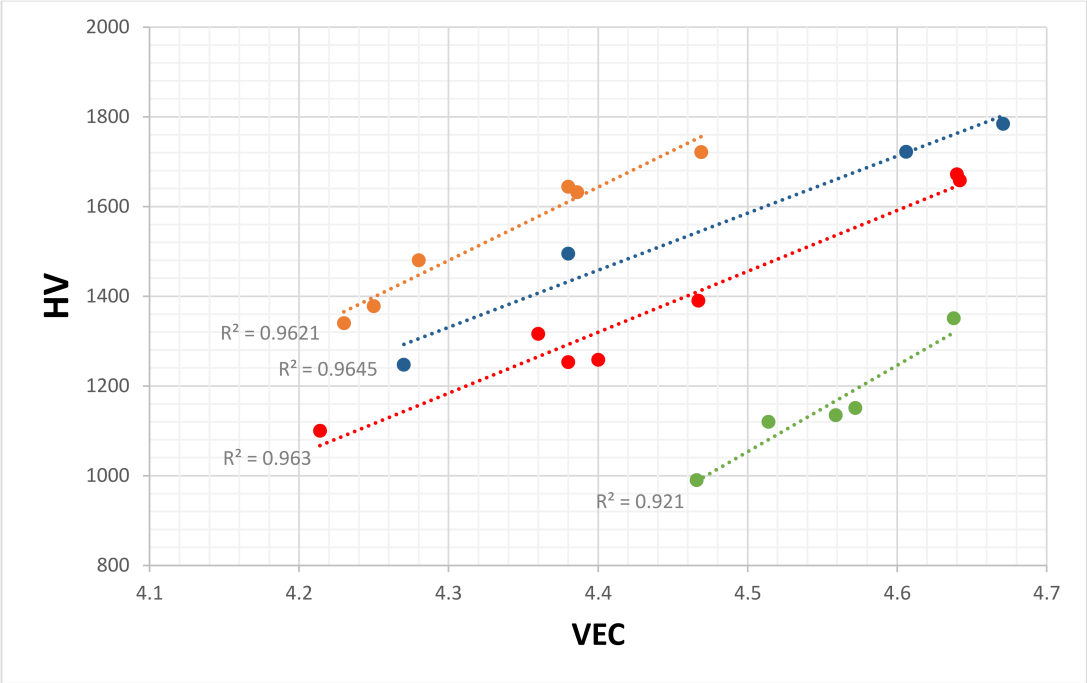


**Figure 13.** Average Vickers hardness of tetragonal $Nb_5Si_3$ silicides (not in eutectics) versus their VEC values. Alloying element additions in series a ($R^2$ = 0.9621) are Al, B, Cr, Ge, Hf, Si, Sn, Ta, and Ti; the alloying element additions in series b ($R^2$ = 0.9645) are Al, B, Cr, Ge, Hf, Si, and Ti; the alloying element additions in series c ($R^2$ = 0.963) are Al, B, Cr, Ge, Hf, Mo, Si, Sn, Ta, Ti, and V; and the alloying element additions in series d ($R^2$ = 0.921) are Al, Cr, Hf, Si, Sn, Ti, V, and W.

The data for the alloys with A15-$Nb_3Sn$ in Figure 12 falls on the same line as the data for the eutectics with only $Nb_{ss}$ and $Nb_5Si_3$, and all of the data exhibits a very good linear fit ($R^2$ = 0.9686). Figure 12b shows that the hardness of the eutectics decreased as their <Si> increased. The linear fit of the hardness versus the <Si> data is also good ($R^2$ = 0.9012), but this was not the case when hardness was plotted against the concentration of Si in the eutectics, which varied from 10.3 at.% to 20 at.% for the alloys in Figure 12.

The ranking of the eutectics in Figure 12 in terms of their hardness from low to high values does not follow the ranking of the hardness of alloyed $Nb_5Si_3$ that was discussed in [39]. Figure 12 suggests that the VEC of the eutectic should decrease as its <Si> content increases. Indeed, this is the case as shown in Figure 14, which also confirms that the data converges to VEC ≈ 4.35 and <Si> ≈ 23 at.%. In Figure 14, there is no Cr in series c, there is no Fe in series c to e, there is no Ge in series e, there is no Mo in series b and e, and there is no Y in series a and c to e. Meanwhile, Ta is present only in series c; V is present only in series a and c; W is present only in series a, c, and d; and Zr is present only in series c. Note the similarities with the data series in Figure 14 and in Figures 6 and 8. The data in Figures 6, 8 and 14 shows that <Si> and $\Delta\chi$ "converge" respectively in the ranges 21.6 at.% to 24.3 at.%, and 0.155 to 0.162.

The hardness of intermetallics has been reported to depend on the scale of their microstructure, and to follow a Hall–Petch relationship [64,65]. Intermetallics participate in eutectics; examples include the $Al/Al_2Cu$, $Al/Al_3Ni$, $Nb/Nb_3Si$, and $Nb/Nb_5Si_3$ eutectics. In a eutectic, the inter-lamellar spacing, the properties of the participating phases, and the interfaces between the lamellae are expected to define their mechanical properties. Refinement of eutectic microstructure can be affected by solidification conditions and/or alloying additions. When the eutectic spacing is refined, the role of interfaces becomes important. Lamellar interfaces are expected to play a major role in the deformation of eutectics.

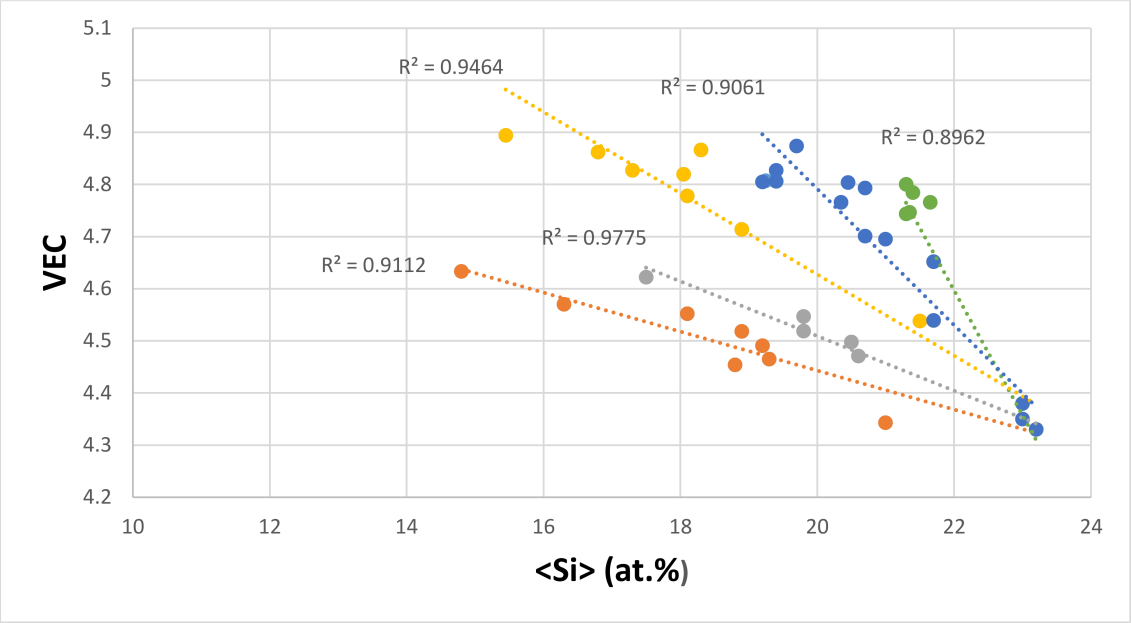


**Figure 14.** VEC versus <Si> map for eutectics with $Nb_{ss}$ and $Nb_5Si_3$ in Nb-silicide based alloys, series a ($R^2$ = 0.9464) with alloying element additions of Al, Cr, Fe, Ge, Hf, Mo, Si, Sn, Ti, V, and W; series b ($R^2$ = 0.9112) with alloying element additions of Al, Cr, Fe, Ge, Hf, Si, Sn, Ti, and Y; series c ($R^2$ = 0.9061) with alloying element additions of Al, Ge, Hf, Mo, Si, Sn, Ta, Ti, V, W, and Zr; series d ($R^2$ = 0.8962) with alloying element additions of Al, Cr, Ge, Hf, Mo, Si, Sn, Ti, and W; series e ($R^2$ = 0.9775) with alloying element additions of Al, Cr, Hf, Si, Sn, and Ti.

The improvement of properties of directionally solidified (DS) eutectics with microstructure refinement has been related to a Hall–Petch relationship for eutectics. For Al–Si eutectics, there are different hardness versus inter-lamellar spacing relationships for different silicon morphologies [66]. Mason et al. showed that the hardness of a $Mo_5Si_3/MoSi_2$ eutectic depended on lamellar spacing in accordance with a Hall–Petch relationship, where the hardness was dependent upon the scale of the lamellae of $MoSi_2$ [67]. Dislocation pile-ups are necessary for Hall–Petch strengthening. Grain boundaries impede dislocation propagation from one grain to the next. As the dislocations pile up against a grain boundary, the stress field assists dislocations to traverse the grain boundary, and thus, deformation spreads from grain to grain. Dislocations are generated during indentation for the measurement of hardness [68]. For the $Mo_5Si_3/MoSi_2$ eutectic, Mason et al. suggested that the $Mo_5Si_3$ silicide behaved as an impenetrable barrier [67].

What is known about the deformation of lamellar microstructures consisting of alloyed $Nb_{ss}$ and $Nb_5Si_3$? How would a strong or weak $Nb_{ss}/Nb_5Si_3$ interface behave under mechanical loading? How important is an orientation relationship between $Nb_{ss}$ and $Nb_5Si_3$ for the deformation of a lamellar $Nb_{ss}/Nb_5Si_3$ structure? Does the morphology of $Nb_5Si_3$ depend on alloying additions? To answer these questions, we need to consider first microstructures based on the Nb–Si binary phase diagram, and then Nb–Si-based (i.e., alloyed) microstructures. Research on the deformation of Nb in $Nb/Nb_5Si_3$ micro-laminate Nb–Si binary foils [69] has highlighted the importance of layer thickness and confirmed that the deformation of Nb was dependent on the thickness of its layers in the foils. As the thickness of the latter increased, their fracture changed from ductile to brittle. This change in fracture mode was attributed to the constraint of Nb and/or changes of crack propagation rate [69]. The hardness of the Nb layers in the micro-laminate foils was 5.4 GPa, which is very close to the hardness of the 1-μm thick Nb thin films that were reported in [70], and significantly higher than the hardness of about 1.6 GPa of about 13-μm Nb particles. The high hardness of the Nb layers was attributed to "their small grain size and the narrow spaced $Nb_5Si_3$ layers, both of which acted to

restrain dislocation motion in the Nb layers" [69]. Gavens et al. also reported that the estimated high average fracture strength of $Nb_5Si_3$ was typical of that of high strength ceramic fibres [69].

A study of a $Nb_{(001)}/\alpha Nb_5Si_{3(001)}$ interface using a first-principles calculation showed that some of the Nb atoms at the interface become a part of $Nb_5Si_3$, and that the Nb–Si bonds at the interface are the likely sites for micro-cracking [71]. This study reported that the work of adhesion and fracture energy of the $Nb_{(001)}/\alpha Nb_5Si_{3(001)}$ interface were 4.4 $J/m^2$ and 33.7 $J/m^2$, respectively.

In Nb-silicide based alloys, both the $Nb_{ss}$ and the $Nb_5Si_3$ are alloyed, and the $Nb_{ss}/Nb_5Si_3$ interface can be Ti-rich (see Section 2). Also, alloying can affect the morphology of $Nb_5Si_3$, whose cross-sections can change from circular to polygonal as the entropy of fusion of $Nb_5Si_3$ increases, owing to alloying additions. The mechanical properties of $[Nb_{ss}]_{(002)}$ /$[\alpha Nb_5Si_3]_{(002)}$ interfaces in a directionally solidified Nb-silicide based alloy of nominal composition Nb-24Ti-15Si-4Cr-2Al-2Hf (at.%) were studied experimentally, and with finite element modelling by Guan et al. [72]. The lower work of the adhesion and fracture energy values compared with the work of Shang et al. [71] were attributed to the alloying of the $[Nb_{ss}]_{(002)}/[\alpha Nb_5Si_3]_{(002)}$ interface, as the latter would be expected to be rich in Ti and Hf on the silicide side and Ti, Hf, Al and Cr on the Nb side, and the different orientation relationship of the studied interface.

The data in Figure 12 is not for the same eutectic of one specific alloy composition, but for different eutectics with $Nb_{ss}$ and $Nb_5Si_3$ in different alloys. In the latter, the phases that participated in the eutectics had different chemical compositions and different hardness, and the eutectics had similar inter-lamellar spacing, but not the same volume fractions of phases and different $Nb_{ss}/Nb_5Si_3$ interface chemistries. Yet, the hardness versus the VEC data for the eutectics of these different alloys followed a remarkable linear relationship with a very good $R^2$ value (=0.9686). This strong relationship is attributed to the covalent bonded intermetallic phase(s) in the eutectics, which are suggested to be the key phases that determine the hardness of the eutectics.

In the solid solution, the bonding is delocalized, and the hardness depends on grain size, grain boundaries, and contamination by interstitials (impurities). In covalent compounds, the mobilities of dislocations are low because of the localized bonding [73]. The dependence of the hardness of covalent bonded hard materials on their shear modulus is stronger than the relationship between the hardness and their bulk modulus [74]. The latter measures the resistance to volume change, which is not the case with the hardness test, and the former is a measure of the rigidity against shape change in the hardness test. Among the various shear stiffnesses, only $C_{44}$ represents a shape change without volume change. Thus, $C_{44}$ provides direct information about the electronic response to shear strain [75]. Jhi et al. [75] showed that there exists a relationship between $C_{44}$ and VEC, and hardness and VEC for different transition metal carbonitrides. For each carbonitride, the trend in the aforementioned relationships was the same, the $C_{44}$ and hardness increased with decreasing VEC to a maximum value for VEC of about 8.4. Wang and Zhou [75] showed that the $C_{44}$ of $M_2AlC$ increased with increasing VEC in the order M = Ti, Nb, V, and Cr. The polynomial fit of the data indicated a maximum value of $C_{44}$ for a VEC of about 8.5. It was also suggested that the hardness of $M_2AlC$ compounds could be predicted from the correlation between $C_{44}$ and VEC [76].

Figures 15 and 16 respectively show the C44 and VEC, and hardness and VEC relationships for $\alpha(Nb,Ti)_5Si_3$ and $\beta(Nb,Ti)_5Si_3$ for Ti = 0, 3.125, 6.25, 9.375, and 12.5 at.% using data for $C_{44}$ from [77]. Unfortunately, there is no experimental data for the hardness of $(Nb,Ti)_5Si_3$ silicides. In [39], it was shown that the hardness values that were calculated using the equation $HV = 2[(G/B)^2G]^{0.585} - 3$ were in better agreement with the available experimental data. The calculations of the hardness values in Figures 15 and 16 used the above equation with data for shear G and bulk B moduli from [77]. Figure 15b shows that the hardness of $\alpha(Nb,Ti)_5Si_3$ increases as the Ti concentration increases and the VEC decreases. Figure 16b shows that the hardness of $\beta(Nb,Ti)_5Si_3$ decreases as the Ti concentration decreases and the VEC increases. The polynomial fit of the data in Figures 15 and 16a showed respectively for $\alpha(Nb,Ti)_5Si_3$ and $\beta(Nb,Ti)_5Si_3$ maximum and minimum values of $C_{44}$ for essentially the same VEC (4.426 and 4.429, respectively). Figure 15 shows that the trends between the $C_{44}$

and VEC and hardness and VEC of $\alpha(Nb,Ti)_5Si_3$ are the same as those reported for transition metal carbonitrides [75]. The trend between the $C_{44}$ and VEC of $\beta(Nb,Ti)_5Si_3$ is the same as that reported for $M_2AlC$ compounds [76]. It should be noted that the trend between hardness and VEC is the same in Figures 12a and 16b; the hardness increases as the VEC increases. Figure 16b is for $\beta(Nb,Ti)_5Si_3$. The $\beta Nb_5Si_3$ is the 5-3 silicide in the metastable eutectic (see Introduction).

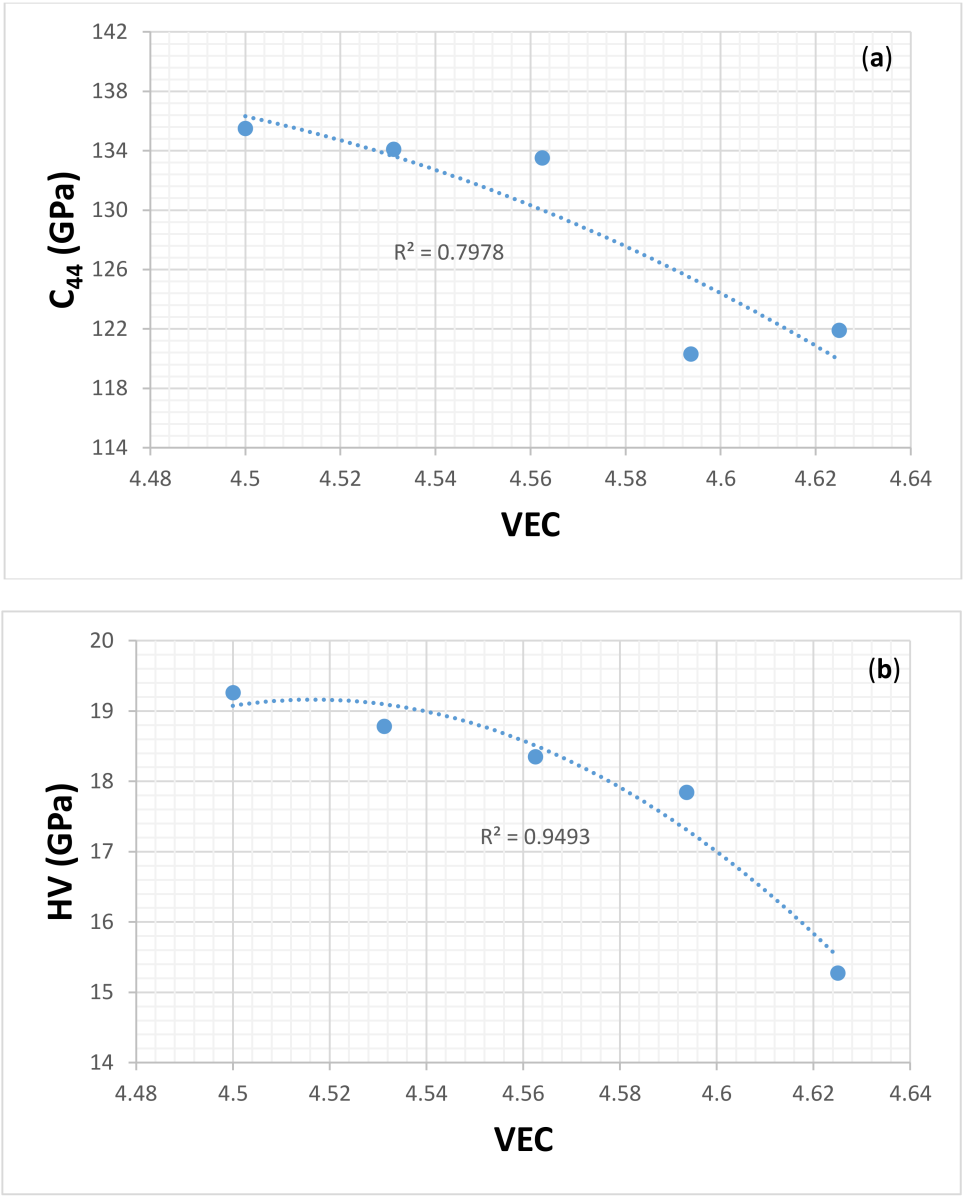


**Figure 15.** (**a**) $C_{44}$ versus VEC and (**b**) calculated hardness versus VEC of $\alpha(Nb,Ti)_5Si_3$.

The eutectics in Figure 12 had 5-3 silicides where only Si was substituted by other simple metal and metalloid elements. There is no $C_{44}$ data for these alloyed silicides. It is suggested that their $C_{44}$ also correlates with VEC. It would be interesting to compare their $C_{44}$ versus VEC and hardness versus the VEC correlations with those of $(Nb,Ti)_5Si_3$ silicides.

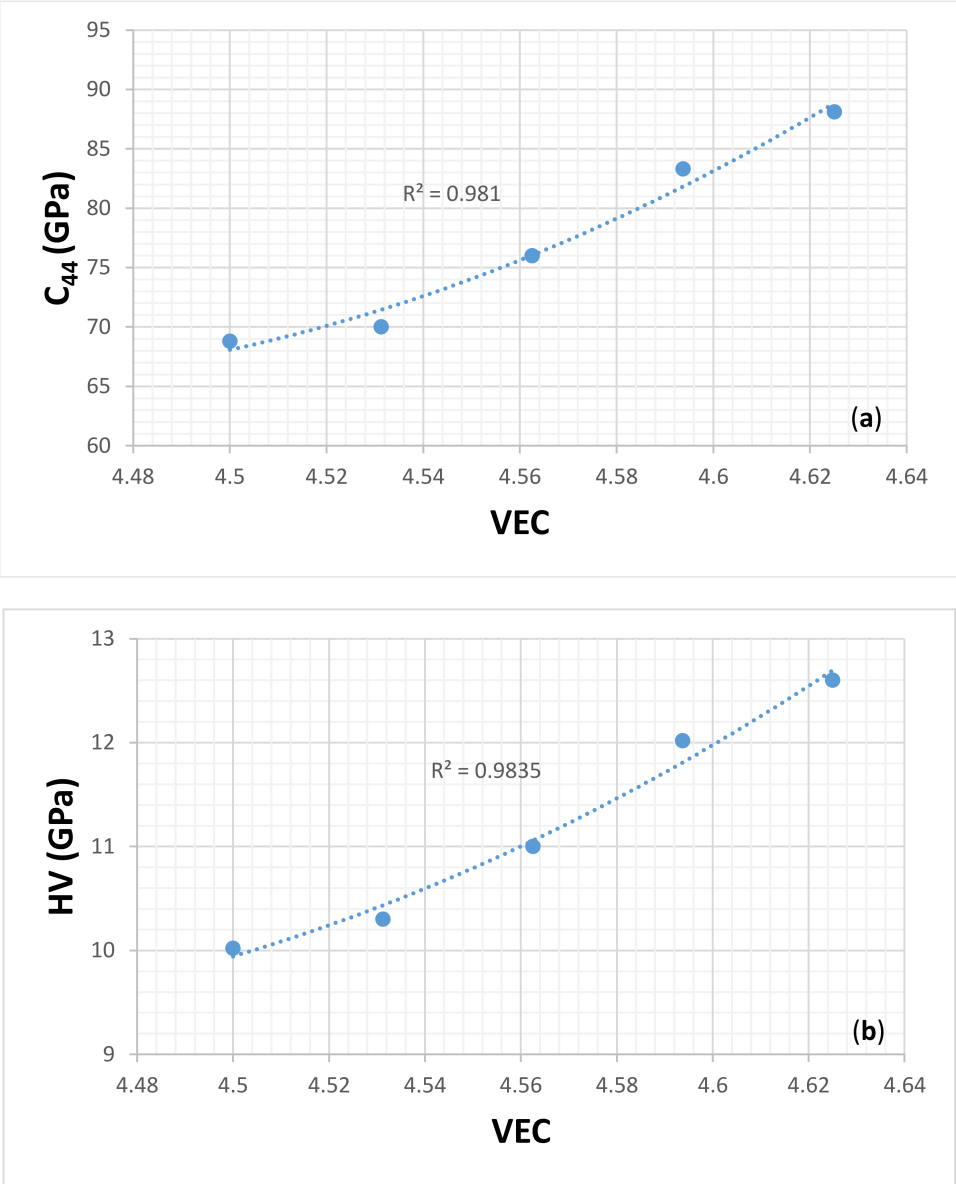


**Figure 16.** (**a**) $C_{44}$ versus VEC and (**b**) calculated hardness versus VEC of $\beta(Nb,Ti)_5Si_3$.

## 4. Conclusions

In Nb-silicide based alloys, eutectics that contain $Nb_{ss}$ and $Nb_5Si_3$ can form. It was shown that the alloying behaviour of the eutectics, the great majority of which are binary $Nb_{ss}$ + $Nb_5Si_3$ eutectics, can be described using the parameters $\Delta H_{mix}$, $\Delta S_{mix}$, VEC, $\delta$, $\Delta\chi$, and $\Omega$.

The values of these parameters were in the ranges $-41.9 < \Delta H_{mix} < -25.5$ kJ/mol, $4.7 < \Delta S_{mix} < 15$ J/molK, $4.33 <$ VEC $< 4.89$, $6.23 < \delta < 9.44$, $0.38 < \Omega < 1.35$, and $0.118 < \Delta\chi < 0.248$, with a gap in the $\Delta\chi$ values between 0.164 and 0.181.

Compared with Nb-silicide based alloys, the eutectics had wider ranges of $\Delta H_{mix}$, $\Delta S_{mix}$, $\Delta\chi$, and $\Omega$ values, the VEC range was essentially the same, the range of $\delta$ values was narrow, and some eutectics had $\delta$ values lower than the Nb-silicide based alloys.

Compared with Nb solid solutions, the eutectics had more negative $\Delta H_{mix}$ values within a wider range; the range of $\Delta S_{mix}$ values was slightly wider; the ranges of the VEC, $\Delta\chi$, and $\delta$ values were narrow; and in the ranges of the values of $Nb_{ss}$ in the Nb-silicide based alloys, the $\Omega$ values were smaller, and outside the range of the $\Omega$ values of the solid solution.

There were correlations between $\Delta S_{mix}$, $\Omega$, $\Delta S_{mix}$, and VEC for all of the eutectics. The correlation between $\Delta H_{mix}$ and $\delta$ was the same as that of the $Nb_{ss}$.

Specific maps of the studied parameters could describe the alloying of the eutectics. The $\delta$ versus $\Delta\chi$ map separated the Ti-rich from the Ti-poor eutectics, with a gap in $\Delta\chi$ values between 0.164 and 0.181, which is within the $\Delta\chi$ gap of the $Nb_{ss}$. Eutectics were also separated according to alloying element additions in the $\Delta\chi$ versus VEC, $\Delta\chi$ versus <Si>, $\delta$ versus <Si>, and VEC versus <Si> maps where <Si> = Al + Ge + Si + Sn.

The convergence of data in maps indicated that (i) the eutectics had $\delta \approx 9.25$ and VEC $\approx 4.35$ and $\Delta\chi$ in the range $\approx 0.155$ to 0.162, and <Si> in the range $\approx 21.6$ at.% to $\approx 24.3$ at.%, (ii) the minimum concentration of Ti, and maximum concentrations of Al and Si in the eutectic were about 8.7 at.% Ti, and 6.3 at.% Al and 21.6 at.% Si, respectively and (iii) the minimum concentration of Si in the eutectic was in the range 8 < Si < 10 at.%.

**Acknowledgments:** The support of the University of Sheffield, EPSRC (GR/R09367, GR/S81759, EP/H500405/1, EP/L026678/1) and Rolls-Royce Plc and discussions with all the members (current and past) of the research group are gratefully acknowledged.

**Conflicts of Interest:** The author declares no conflict of interest.

## References

1. Bewlay, B.P.; Jackson, M.R.; Gigliotti, M.F.X. Niobium Silicide High Temperature In-Situ Composites. In *Intermetallic Compounds, Principles and Practice*; Westbrook, J.H., Fleisher, R.L., Eds.; John Wiley and Sons: Chichester, UK, 2001; pp. 541–560.
2. Broutman, L.J.; Krock, H.H. *Modern Composite Materials*; Addison Wesley: Boston, MA, USA, 1967; p. 442.
3. Sharp, R.M.; Flemings, M.C. Growth of composites of off-eutectic alloys. In Proceedings of the Conference In-Situ Composites, Lakeville, CT, USA, 5–8 September 1972; National Materials Advisory Board: Washington, DC, USA, 1972; Volume 1, pp. 51–59.
4. Mollard, F.R.; Flemings, M.C. Growth of composites from melt—Part I. *TMS-AIME* **1967**, *239*, 1534–1539.
5. Yue, A.S.; Kaba, B.D. Fracture behaviour of unidirectionally solidified Ti-$Ti_5Si_3$ eutectic composites. *ASTM STP* **1975**, *580*, 504–514.
6. Crossman, F.W.; Yue, A.S. Unidirectionally solidified Ti-TiB and Ti-$Ti_5Si_3$ eutectic composites. *Metall. Trans.* **1971**, *2*, 1545–1555.
7. Jehanno, P.; Heilmaier, M.; Kestler, H.; Boning, M.; Venskutonis, A.; Bewlay, B.; Jackson, M. Assessment of a powder metallurgical route for refractory metal silicide alloys. *Metall. Mater. Trans. A* **2005**, *36*, 515–523. [CrossRef]
8. Schlesinger, M.E.; Okamoto, H.; Gokhale, A.B.; Abbaschian, R. The Nb-Si (Niobium-Silicon) system. *J. Phase Equilib.* **1993**, *14*, 502–5099. [CrossRef]
9. Bewlay, B.P.; Lipsitt, H.A.; Reeder, W.J.; Jackson, M.R.; Sutliff, J.A. Toughening mechanisms in directionally solidified Nb-$Nb_3Si$-$Nb_3Si_5$ in-situ composites. In *Processing and Fabrication of Advanced Materials III*; Ravi, V.A., Srivatsan, T.S., Moore, J.J., Eds.; The Minerals Metals and Materials Society: Warrendale, PA, USA, 1994; pp. 547–565.
10. Yuan, S.; Jia, L.; Ma, L.; Cui, R.; Su, L.; Zhang, H. The microstructure optimising of the Nb-14Si-22Ti-4Cr-2Al-2Hf alloy processed by directional solidification. *Mater. Lett.* **2012**, *84*, 124–127. [CrossRef]
11. Su, L.; Jia, L.; Feng, Y.; Zhang, H.; Yuan, S.; Zhang, H. Microstructure and room temperature fracture toughness of directionally solidified Nb-Si-Ti-Cr-Al-Hf alloy. *Mater. Sci. Eng. A* **2013**, *560*, 672–677. [CrossRef]
12. Wang, J.; Jia, L.; Ma, L.; Yuan, S.; Zhang, X.; Zhang, H. Microstructure optimisation of directionally solidified hypereutectic Nb-Si alloy. *Trans. Nonferr. Met. Soc. China* **2013**, *23*, 2874–2881. [CrossRef]
13. Weng, J.F.; Jia, L.N.; Yuan, S.N.; Su, L.F.; Ding, F.; Zhang, H. Microstructure evolution of directionally solidified Nb-Si alloy. *Mater. Sci. Technol.* **2014**, *30*, 418–423. [CrossRef]
14. Guo, H.; Guo, X. Microstructure evolution and room temperature fracture toughness of an integrally directionally solidified Nb-Ti-Si based ultrahigh temperature alloy. *Scr. Mater.* **2011**, *64*, 637–640. [CrossRef]

15. Yuan, S.N.; Jia, L.N.; Su, L.F.; Ma, L.M.; Zhang, H. Microstructure evolution and solidification behaviour of Nb-16Si-22Ti-2Cr-2Al-6Hf alloy processed by directional solidification. *Mater. Res. Innov.* **2013**, *17*, 184–188. [CrossRef]
16. Guo, B.H.; Guo, X.P. Microstructure of Nb-Ti-Si based ultrahigh temperature alloy processed by integrally directional solidification. *Mater. Sci. Technol.* **2015**, *31*, 231–236. [CrossRef]
17. Sekido, N.; Kimura, Y.; Miura, S.; Wei, F.; Mishima, Y. Fracture toughness and high temperature strength of unidirectionally solidified Nb-Si binary and Nb-Ti-Si ternary alloys. *J. Alloys Compd.* **2006**, *425*, 223–229. [CrossRef]
18. Sekido, N.; Kimura, Y.; Miura, S.; Mishima, Y. Microstructure development of unidirectionally solidified (Nb)/$Nb_3Si$ eutectic alloys. *Mater. Sci. Eng. A* **2007**, *444*, 51–57. [CrossRef]
19. Hunag, Q.; Guo, X.; Kang, Y.; Song, J.; Qu, S.; Han, Y. Microstructures and mechanical properties of directionally solidified multi-element Nb-Si alloy. *Prog. Nat. Sci. Mater. Int.* **2011**, *21*, 146–152. [CrossRef]
20. Cheng, G.M.; He, L.L. Microstructure evolution and room temperature deformation of a unidirectionally solidified Nb-22Ti-16Si-3Ta-2Hf-7Cr-3Al-0.2Ho (at.%) alloy. *Intermetallics* **2011**, *19*, 196–201. [CrossRef]
21. Li, Y.; Miura, S.; Ohsasa, K.; Ma, C.; Zhang, H. Ultra-high temperature $Nb_{ss}/Nb_5Si_3$ fully lamellar microstructure developed by directional solidification in OFZ furnace. *Intermetallics* **2011**, *19*, 460–469. [CrossRef]
22. McCaughey, C. The Solidification of Niobium Silicides for Next Generation Gas Turbine Engines. Ph.D. Thesis, University of Sheffield, Sheffield, UK, 2016.
23. Bendersky, L.; Biancaniello, F.S.; Boettinger, W.J.; Perepezko, J.H. Microstructural characterisation of rapidly solidified Nb-Si alloys. *Mater. Sci. Eng.* **1987**, *89*, 151–159. [CrossRef]
24. Abbaschian, R.; Lipschutz, M.D. Eutectic solidification processing via bulk melt undercooling. *Mater. Sci. Eng. A* **1997**, *226–228*, 13–21. [CrossRef]
25. Wang, Y.; Dong, S.; Wei, B.; Li, W. Undercooling and rapid solidification of Nb-Si eutectic alloys studied by long drop tube. *Trans. Nonferr. Met. Soc. China* **2006**, *16*, s89–s92.
26. Liang, H.; Chang, Y.A. Thermodynamic modelling of the Nb-Si-Ti ternary system. *Intermetallics* **1999**, *7*, 561–570. [CrossRef]
27. Okamoto, H.; Gokhale, A.B.; Abbaschian, G.J. *Binary Phase Diagrams*, 2nd ed.; Massalski, T.B., Ed.; ASM International: Materials Park, OH, USA, 1990; pp. 2764–2768.
28. Okamoto, H. *Phase Diagrams for Binary Alloys: Desk Handbook*; ASM International: Metals Park, OH, USA, 2000.
29. Fernandes, P.B.; Coelho, G.C.; Ferreira, F.; Nunes, C.A.; Sudman, B. Thermodynamic modelling of the Nb-Si system. *Intermetallics* **2002**, *10*, 993–999. [CrossRef]
30. *ASM Alloy Phase Diagram Database*; Villars, P.; Okamoto, H.; Cenzual, K. (Eds.) ASM International: Materials Park, OH, USA, 2016.
31. Geng, T.; Li, C.; Bao, J.; Zhao, X.; Du, Z.; Guo, C. Thermodynamic assessment of the Nb-Si-Ti system. *Intermetallics* **2009**, *17*, 343–357. [CrossRef]
32. Li, Y.; Li, C.; Du, Z.; Guo, C.; Zhao, X. As-cast microstructures and solidification paths of the Nb-Si-Ti ternary alloys in $Nb_5Si_3$–$Ti_5Si_3$ region. *Rare Met.* **2015**, *32*, 502–511. [CrossRef]
33. Gigolotti, J.C.J.; Coelho, G.C.; Nunes, C.A.; Suzuki, P.A.; Joubert, J. Experimental evaluation of the Nb-Si-Ti system from as-cast alloys. *Intermetallics* **2017**, *82*, 76–92. [CrossRef]
34. Goldschmidt, H.J.; Brand, J.A. The constitution of the chromium–niobium–silicon system. *J. Less-Common Met.* **1961**, *3*, 34–43. [CrossRef]
35. Zhao, C.; Jackson, M.R.; Peluso, L.A. Determination of the Nb-Cr-Si phase diagram using diffusion multiples. *Acta Mater.* **2003**, *51*, 6395–6405. [CrossRef]
36. Geng, J.; Shao, G.; Tsakiropoulos, P. Study of three-phase equilibrium in the Nb rich corner of Nb-Si-Cr system. *Intermetallics* **2006**, *14*, 832–837. [CrossRef]
37. Bewlay, B.P.; Yang, Y.; Casey, R.L.; Jackson, M.R.; Chang, Y.A. Experimental study of the liquid-solid phase equilibria at the metal rich region of the Nb-Cr-Si system. *Intermetallics* **2009**, *17*, 120–127. [CrossRef]
38. Tsakiropoulos, P. On the Nb silicide based alloys: Part I—The bcc Nb solid solution. *J. Alloys Compd.* **2017**, *708*, 961–971. [CrossRef]
39. Tsakiropoulos, P. On the alloying and properties of tetragonal $Nb_5Si_3$ in Nb-silicide based alloys. *Materials* **2018**, *11*, 69. [CrossRef] [PubMed]

40. Grammenos, I.; Tsakiropoulos, P. Study of the role of Al, Cr and Ti additions in the microstructure of Nb-18Si-5Hf base alloys. *Intermetallics* **2010**, *18*, 242–253. [CrossRef]
41. Grammenos, I.; Tsakiropoulos, P. Study of the role of Mo and Ta additions in the microstructure of Nb-18Si-5Hf silicide based alloys. *Intermetallics* **2010**, *18*, 1524–1530. [CrossRef]
42. Grammenos, I.; Tsakiropoulos, P. Study of the role of Hf, Mo and W additions in the microstructure of Nb-20Si silicide based alloys. *Intermetallics* **2011**, *19*, 1612–1621. [CrossRef]
43. Vellios, N.; Tsakiropoulos, P. The role of Sn and Ti additions in the microstructure of Nb-18Si based alloys. *Intermetallics* **2007**, *15*, 1518–1528. [CrossRef]
44. Vellios, N.; Tsakiropoulos, P. The role of Fe and Ti additions in the microstructure of Nb-18Si-5Sn silicide based alloys. *Intermetallics* **2007**, *15*, 1529–1537. [CrossRef]
45. Li, Z.; Tsakiropoulos, P. Study of the effects of Ge addition on the microstructure of Nb-18Si in situ composites. *Intermetallics* **2010**, *18*, 1072–1078.
46. Li, Z.; Tsakiropoulos, P. Study of the effect of Ti and Ge in the microstructure of Nb-24Ti-18Si-5Ge in situ composite. *Intermetallics* **2011**, *19*, 1291–1297. [CrossRef]
47. Li, Z.; Tsakiropoulos, P. Study of the effect of Cr and Ti additions in the microstructure of Nb-18Si-5Ge based in situ composites. *Intermetallics* **2012**, *26*, 18–25. [CrossRef]
48. Li, Z.; Tsakiropoulos, P. The microstructures of Nb-18Si-5Ge-5Al and Nb-24Ti-18Si-5Ge-5Al in situ composites. *J. Alloys Compd.* **2013**, *550*, 553–560. [CrossRef]
49. Zacharis, E.; Tsakiropoulos, P. Development of N Silicide Based Alloys with Hf and Sn Additions. University of Sheffield: Sheffield, UK, Unpublished Research. 2013.
50. Zhao, J. The Role of Refractory Metals in Controlling Properties of Nb-silicide Based In Situ Composites. Ph.D. Thesis, University of Sheffield, Sheffield, UK, 2017.
51. Xu, Z. The Effect of Sn on the Phase Stability and Oxidation Behaviour of Nb-silicide Based Alloys. Ph.D. Thesis, University of Sheffield, Sheffield, UK, 2016.
52. Vellios, N.; Tsakiropoulos, P. Nb-silicide Based Alloys with Sn and Fe Additions. University of Surrey: Guildford, UK, Unpublished Research. 2007.
53. Anazodo, B.; Tsakiropoulos, P. Nb-Si Alloys with Refractory Metal and Metalloid Element Additions. University of Sheffield: Sheffield, UK, Unpublished Research. 2013.
54. Ghadyani, M. Study of the Microstructure and Oxidation of Alloys on the Al-Hf-Nb-Si-Ti System. Ph.D. Thesis, University of Sheffield, Sheffield, UK, 2017.
55. Tweddle, A.; Tsakiropoulos, P. Nb-Si Based Alloys with Ge Additions. University of Sheffield: Sheffield, UK, Unpublished Research. 2015.
56. Nelson, J. Study of the Effects of Cr, Hf and Sn with Refractory Metal Additions on the Microstructure and Properties of Nb-silicide Based Alloys. Ph.D. Thesis, University of Sheffield, Sheffield, UK, 2015.
57. Kim, W.; Tanaka, H.; Kasama, A.; Hanada, S. Microstructure and room temperature fracture toughness of $Nb_{ss}/Nb_5Si_3$ in situ composites. *Intermetallics* **2001**, *9*, 827–834. [CrossRef]
58. Kashyap, S.; Tiwary, C.S.; Chattopadhyay, K. Effect of Gallium on microstructure and mechanical properties of Nb-Si eutectic alloy. *Intermetallics* **2011**, *19*, 1943–1952. [CrossRef]
59. Zelenitsas, K.; Tsakiropoulos, P. Study of the role of Al and Cr additions in the microstructure of Nb-Ti-Si in situ composites. *Intermetallics* **2005**, *13*, 1079–1095. [CrossRef]
60. Zelenitsas, K.; Tsakiropoulos, P. Study of the role of Ta and Cr additions in the microstructure of Nb-Ti-Si-Al in situ composites. *Intermetallics* **2006**, *14*, 639–659. [CrossRef]
61. Grammenos, I.; Tsakiropoulos, P. Development of Creep Resistant Nb Silicide Based Alloys. University of Surrey: Guildford, UK, Unpublished Research. 2007.
62. Tsakiropoulos, P. On Nb silicide based alloys: Part II. *J. Alloys Compd.* **2018**, *748*, 569–576. [CrossRef]
63. Tsakiropoulos, P. Alloying and properties of C14-$NbCr_2$ and A15-$Nb_3X$ (X = Al, Ge, Si, Sn) in Nb-silicide based alloys. *Materials* **2018**, *11*, 395. [CrossRef] [PubMed]
64. Westbrook, J.H. *Intermetallic Compounds*; R E Krieger Publishing Company: New York, NY, USA, 1997; p. 471.
65. Tiwari, R.; Herman, H.; Sampath, S. Vacuum plasma spraying of $MoSi_2$ and its composites. *Mater. Sci. Eng. A* **1992**, *155*, 95–100. [CrossRef]
66. Yilmaz, F.; Elliot, R. The microstructure and mechanical properties of unidirectionally solidified Al-Si alloys. *J. Mater. Sci.* **1989**, *24*, 2065–2070. [CrossRef]

67. Mason, D.P.; van Aken, D.C. The effect of microstructural scale on hardness of $MoSi_2$-$Mo_5Si_3$ eutectics. *Scr. Met.* **1993**, *28*, 185–189. [CrossRef]
68. Boldt, P.H.; Embury, J.D.; Weatherly, G.C. Room temperature micro-indentation of single crystal $MoSi_2$. *Mater. Sci. Eng. A* **1992**, *155*, 251–258. [CrossRef]
69. Gavens, A.J.; van Heerden, D.; Foecke, T.; Weihs, T.P. Fabrication and evaluation of $Nb/Nb_5Si_3$ micro-laminate foils. *Metall. Mater. Trans. A* **1999**, *30*, 2959–2965. [CrossRef]
70. Ji, H.; Was, G.S.; Jones, J.W. Layered Materials for Structural, Applications. In Proceedings of the Materials Research Society Symposia, San Francisco, CA, USA, 8–10 April 1996; Materials Research Society: Pittsburgh, PA, USA, 1996; Volume 434, pp. 153–158.
71. Shang, J.X.; Guan, K.; Wang, F.H. Atomic structure and adhesion of the $Nb_{(001)}/\alpha Nb_5Si_{3(001)}$ interface: A first-principles study. *J. Phys. Condens. Matter.* **2010**, *22*, 085004. [CrossRef] [PubMed]
72. Guan, K.; Jia, L.; Kong, B.; Yuan, S.; Zhang, H. Improvement of fracture toughness of directionally solidified Nb-silicide in situ composites using artificial neural network. *Mater. Sci. Eng. A* **2016**, *663*, 98–107. [CrossRef]
73. Gilman, J.J. Physical chemistry of intrinsic hardness. *Mater. Sci. Eng. A* **1996**, *209*, 74–81. [CrossRef]
74. Teter, D.M. Computational alchemy: The search for new superhard materials. *MRS Bull.* **1998**, *23*, 22–27. [CrossRef]
75. Jhi, S.; Ihm, J.; Loule, S.G.; Cohen, M.L. Electronic mechanism of hardness enhancement in transition-metal carbo-nitrides. *Nature* **1999**, *399*, 132–134. [CrossRef]
76. Wang, J.; Zhou, Y. Dependence of elastic stiffness on electronic band structure of nanolaminate $M_2AlC$ (M = Ti, V, Nb and Cr) ceramics. *Phys. Rev. B* **2004**, *69*, 214111. [CrossRef]
77. Papadimitriou, I.; Utton, C.; Tsakiropoulos, P. The impact of Ti and temperature on the stability of $Nb_5Si_3$ phases: A first-principles study. Sci. Technol. *Adv. Mater.* **2017**, *18*, 467–479. [CrossRef] [PubMed]